

Metal Enrichment and Ionization Balance in the Lyman α Forest at $z = 3$.

Antoinette Songaila¹ & Lennox L. Cowie¹

Institute for Astronomy, University of Hawaii, 2680 Woodlawn Dr., Honolulu, HI 96822

Accepted for publication in *Astronomical Journal*, May 14, 1996

Received _____; accepted _____

¹The authors were visiting astronomers at the W. M. Keck Observatory, jointly operated by the California Institute of Technology and the University of California. The research was supported at the University of Hawaii by the State of Hawaii.

ABSTRACT

The recent discovery of carbon in close to half of the low neutral hydrogen column density [$N(\text{H I}) > 3 \times 10^{14} \text{ cm}^{-2}$] Lyman forest clouds toward $z \sim 3$ quasars has challenged the widely held view of this forest as a chemically pristine population uniformly distributed in the intergalactic medium, but has not eliminated the possibility that a primordial population might be present as well. Using extremely high signal-to-noise observations of a sample of quasars we now show that C IV can be found in 75% of clouds with $N(\text{H I}) > 3 \times 10^{14} \text{ cm}^{-2}$ and more than 90% of those with $N(\text{H I}) > 1.6 \times 10^{15} \text{ cm}^{-2}$. Clouds with $N(\text{H I}) > 10^{15} \text{ cm}^{-2}$ show a narrow range of ionization ratios, spanning less than an order of magnitude in C IV/H I, C II/C IV, Si IV/C IV and N V/C IV, and their line widths require that they be photoionized rather than collisionally ionized. This in turn implies that the systems have a spread of less than an order of magnitude in both volume density and metallicity. Carbon is seen to have a typical abundance of very approximately 10^{-2} of solar and Si/C about three times solar, so that the chemical abundances of these clouds are very similar to those of Galactic halo stars. Si IV/C IV decreases rapidly with redshift from high values (> 0.1) at $z > 3.1$, a circumstance which we interpret as a change in the ionizing spectrum as the intergalactic medium becomes optically thin to He^+ ionizing photons. Weak clustering is seen in the C IV systems for $\Delta v < 250 \text{ km sec}^{-1}$, which we argue provides an upper limit to the clustering of H I clouds. If the clouds are associated with galaxies, this requires a rapid evolution in galaxy clustering between $z = 3$ and $z = 0$.

1. Introduction

A clear theoretical paradigm is beginning to emerge in which the forest of Ly α absorption lines seen in quasar spectra is interpreted in terms of the development of structure in the intergalactic gas (Cen et al. 1994). This model subsumes many aspects of previous models (Rees 1995) but places the observations in the much broader intellectual context of the formation of galaxies and large scale structure and of the evolution of the intergalactic medium as a whole.

This type of model has considerable predictive power and it is already clear that it can explain in broad terms the hydrogen properties of the forest clouds — that is, the column density distribution, b -values and turbulence of the Ly α forest lines (Zhang, Anninos & Norman 1996) but, given the uncertainties in cosmology, the perturbation spectrum and the evolution of the ionizing field, the coarse information available in the H I data may not sufficiently challenge the theory. However, the models also make detailed predictions of the ionization balance (collisional and photoionization) in heavier elements (Haehnelt et al. 1996) that are now testable with the detection of metals in many forest clouds (Cowie et al. 1995 [Paper I], Tytler et al. 1995).

The presence of metals is also of considerable interest in itself. If forest clouds are associated with galaxies, large radii ($\sim 200h^{-1}$ kpc) are required to account for the number density of $N(\text{H I}) > 10^{15}$ cm $^{-2}$ clouds at $z = 3$, and it appears unlikely that star formation in the galaxy itself could contaminate this entire region. The remaining possibilities would seem to be that the metals are being produced by *in situ* star formation in the clouds themselves, perhaps as an early stage in the galaxy formation process, or that they are formed in an even earlier stage of metal production at much higher redshift that has uniformly enhanced the intergalactic medium. Since this latter (Population III) process presumably would occur on a sub-galactic scale, we might expect it to produce a more uniform metallicity at the scale

of the clouds than *in situ* star formation would produce; in contrast, we would expect *in situ* enrichment to depend heavily on the properties of individual clouds and perhaps to be strongest in higher density clouds.

We shall show in this paper that $N(\text{C IV}) \geq 10^{12} \text{ cm}^{-2}$ in 90% of clouds with $N(\text{H I}) > 1.6 \times 10^{15} \text{ cm}^{-2}$ and $N(\text{C IV}) \geq 5 \times 10^{11} \text{ cm}^{-2}$ in 75% of clouds with $N(\text{H I}) > 3.0 \times 10^{14} \text{ cm}^{-2}$. The fraction of detections is consistent with the hypothesis that all clouds have a uniform distribution of C IV/H I as a function of $N(\text{H I})$, but still leaves open the possibility that as much as 50% of clouds at these column densities may be primordial. The heavy element properties of the $N(\text{H I}) > 10^{15} \text{ cm}^{-2}$ clouds are remarkably uniform and may pose a significant challenge to the structure development models which predict a wide range of densities and temperatures in the clouds. This uniformity also favors the pre-enrichment hypothesis for the origin of the metals.

The forest metal lines also provide excellent probes of the intergalactic ionizing flux and its evolution. Since they are generally weak lines, their column densities can be measured accurately by profile fitting and there are no considerations of neutral hydrogen optical depth as there are for higher column density clouds. We find that there is a significant evolution in SI IV/C IV as a function of redshift, with an abrupt decrease in this quantity at $z < 3.1$. The data can be understood in terms of a photoionization model in which the He^+ edge becomes optically thin below $z = 3.1$. The one cloud close to a quasar ($\Delta v < 1000 \text{ km sec}^{-1}$) is found to have significantly higher ionization parameters but also to have anomalous metallicity, in agreement with the findings of Petitjean, Rauch & Carswell (1994) for higher column density systems.

Finally, we consider the velocity clustering of the C IV systems (e.g. Fernandez-de Soto et al. 1996). The clustering extends to $\Delta v = 250 \text{ km sec}^{-1}$; if forest clouds are assumed to trace galaxy clustering at these redshifts, this requires a rapid evolution in galaxy clustering

from $z = 3$ to $z = 0$.

2. Observations

We draw primarily on two extremely high sensitivity, high resolution ($R = 36,000$) spectra of the $z = 3.4$ quasar Q0014+813, and of the $z = 3.6$ quasar Q1422+231, that we have obtained with the HIRES spectrograph on the Keck 10 m telescope. Total integration times were 7.75 hours on Q0014+813 and 8.3 hours on Q1422+231. In each case the spectrograph was used in three separate configurations to provide complete wavelength coverage of all C IV absorption longward of the Lyman forest as well as the corresponding $\text{Ly}\alpha$ and $\text{Ly}\beta$ portions of the spectra. Q1422+231 is gravitationally lensed but the major components all lie within the $1''.1$ slit used in the observations; the combined source is therefore extremely luminous ($g = 15.8$; Yee & Ellingson 1994) and provided a truly exceptional spectrum, illustrated in Figure 1, with $S/N = 160$ per resolution element in the segment from 6300 \AA to 6400 \AA shown in the upper panel. The spectrum of Q0014+813 has poorer S/N by about, on average, a factor of two. For certain of the measurements, where a larger sample was needed, we included spectra of a larger collection (Songaila 1996) of $z \sim 3$ quasars; this is summarized in the legend of Fig. 4. Details of the reduction process are given in Paper I and Hu et al. (1995), with a more extensive discussion in Songaila (1996).

3. Fractions of C IV Detections in Forest Clouds

3.1. Introduction

In Paper I and Tytler et al. (1995) it was shown that roughly 50% of Ly α forest clouds with $N(\text{H I}) \gtrsim 3 \times 10^{14} \text{ cm}^{-2}$ have C IV absorption with $N(\text{C IV}) > 10^{12} \text{ cm}^{-2}$. A critical question is whether the clouds that are undetected in C IV are simply below the detection limit or whether at these H I column densities there are two classes of forest cloud — one that contains metals and another that is chemically pristine. In order to try to understand this issue we have looked at two further samples. In section 3.2 we consider a higher- $N(\text{H I})$ selection [$N(\text{H I}) \geq 1.6 \times 10^{15} \text{ cm}^{-2}$] and in section 3.3 we use the very sensitive Q1422+231 observations to determine the C IV fraction in a Ly α -selected sample (i.e. $N(\text{H I}) \gtrsim 3 \times 10^{14} \text{ cm}^{-2}$).

3.2. Lyman β selection

For Q1422+231 we first selected all Lyman forest cloud components for which $r_\nu \equiv \exp(-\tau_\nu) \leq 0.02$. Here r_ν is the residual flux at the base of the line and τ_ν is the corresponding optical depth. The search detected 62 clouds in a redshift interval from $z = 2.65$, where C IV lies redward of the Ly α forest, to the quasar’s redshift $z = 3.625$ (Fig. 1). This constitutes the Ly α sample we discuss in the next subsection. Fig. 2 is an atlas of these lines along with the corresponding C IV ($\lambda 1548, 1550 \text{ \AA}$) lines and Ly β (redward of $z = 2.92$; see below).

For clouds with $z > 2.92$ the Lyman β line lies sufficiently redward of the Lyman edge, at 4000 \AA , corresponding to the $z = 3.38$ Lyman limit system, that the signal-to-noise at the Ly β position is adequate for applying our selection criteria, and between here and the quasar redshift we have drawn a subsample of clouds that are saturated in both Ly α and Ly β . This method of selection is illustrated in Fig. 3. The selection chooses clouds that have a higher column density than a Ly α selection would choose, in roughly the ratio ($= 5.2$) of the Ly α to Ly β oscillator strengths; this picks out clouds with $N(\text{H I}) \gtrsim 1.6 \times 10^{15} \text{ cm}^{-2}$ for

b -values typical of forest clouds.

In order to supplement this sample we applied the same procedure to the spectra from six other quasars: these are the four quasars of Paper I plus Q1159+123 and Q2126–158, which were observed subsequently. Except for Q0014+813, these spectra do not extend to the quasars’ C IV emission, and only a narrower redshift range could be used in each case; these redshift ranges are summarised in the legend of Fig. 4.

For each cloud selected, as long as the C IV lay redward of the Ly α forest, the column density of C IV was measured by profile fitting to the C IV 1548 Å and 1550 Å lines. All the lines are unsaturated and there is good agreement between the two members of the doublet. The sensitivity limit for C IV is slightly variable from quasar to quasar, but for $N(\text{C IV}) > 10^{12} \text{ cm}^{-2}$, both members of the doublet can generally be detected at the 2σ level for $b = 10 \text{ km sec}^{-1}$, and we adopt this as our sensitivity limit.

There are 41 clouds in the sample of Ly β -saturated clouds, of which 36 (88%) are detected in C IV. This is shown in Fig. 4 where we plot $N(\text{C IV})$ versus redshift; the undetected systems are shown at $N(\text{C IV}) = 10^{12} \text{ cm}^{-2}$. There is no significant evolution of the $N(\text{C IV})$ distribution as a function of redshift. Some fraction (roughly half) of the 5 systems that are not detected will correspond to false systems, where there is Ly α contamination of the Ly β position, so that the actual detection fraction lies between 90% and 100%. This is our first conclusion: essentially all Ly α forest clouds with $N(\text{H I}) \gtrsim 1.6 \times 10^{15} \text{ cm}^{-2}$ contain metals.

The median column density of the C IV lines is $4.3 \times 10^{12} \text{ cm}^{-2}$, and the mean column density is $1.61 \times 10^{13} \text{ cm}^{-2}$ if the five undetected systems are included at $N(\text{C IV}) = 10^{12} \text{ cm}^{-2}$, and is $1.59 \times 10^{13} \text{ cm}^{-2}$ if these five are assigned zero column density. If we assume that the hydrogen column density distribution is of the form $n(N(\text{H I}))dN \sim N^{-1-\beta}dN$, then, for $\beta = 0.7$, the median $N(\text{H I})$ is $2.6 \times 10^{15} \text{ cm}^{-2}$ and the mean value $9.7 \times 10^{15} \text{ cm}^{-2}$, where we have assumed an upper cutoff value of 10^{17} cm^{-2} in calculating the latter. The ratio of

the medians gives $C\text{ IV}/H\text{ I} = 1.6 \times 10^{-3}$; the ratio of the means gives an identical result.

Figs. 4(b) and (c) show the corresponding diagrams for the Si IV ($\lambda\lambda 1393, 1402\text{ \AA}$) and N V ($\lambda\lambda 1238, 1242\text{ \AA}$) doublets. Because of the short wavelength of N V there is only a very small number of systems that lie redward of the Ly α forest. Fig. 4(d) shows the corresponding diagram for C II ($\lambda 1334.5\text{ \AA}$); since there is no corroborating additional line in this case a small fraction of the detections may be spurious. 38% of the clouds are detected in Si IV and the mean column density lies in the range $(1.5 - 1.8) \times 10^{12}\text{ cm}^{-2}$, depending on whether undetected clouds are given a value of 0 or $5 \times 10^{11}\text{ cm}^{-2}$. The corresponding values for N V are 17% and $(0.2 - 1.1) \times 10^{12}\text{ cm}^{-2}$, and for C II are 24% and $(1.7 - 2.5) \times 10^{12}\text{ cm}^{-2}$. The ratios of these values to that of C IV in the mean are $Si\text{ IV}/C\text{ IV} = [0.09, 0.11]$, $N\text{ V}/C\text{ IV} = [0.01, 0.07]$ and $C\text{ II}/C\text{ IV} = [0.11, 0.16]$.

In contrast to C IV, both the Si IV and C II appear to show a trend to increasing values at higher z . This has been noted previously in studies of equivalent widths of the higher column density metal lines (e.g. Bergeron & Ikeuchi 1990). We will return to this point in the next section.

3.3. Lyman α selection

The extremely high S/N of the Q1422+231 observations has made it possible to search for C IV absorption in the entire Ly α selected sample of Fig. 2 to a considerably lower column density than was possible for the quasars of Paper I. We show $N(C\text{ IV})$ versus redshift for all the Ly α selected clouds in Q1422+231 in Fig. 5, where we have adopted a conservative limit of $N(C\text{ IV}) = 5 \times 10^{11}\text{ cm}^{-2}$ at which both components of the doublet will be detected above the 2σ level.

As with the Ly β -selected sample, there is no obvious trend with redshift. $(75 \pm 10)\%$ of

the clouds (50 out of 75) are detected in C IV with a median $N(\text{C IV}) = 1.4 \times 10^{12} \text{ cm}^{-2}$ and a mean of $[9.5, 9.6] \times 10^{12} \text{ cm}^{-2}$. Assuming a median $N(\text{H I})$ of $5 \times 10^{14} \text{ cm}^{-2}$ and a mean of $4 \times 10^{15} \text{ cm}^{-2}$ we obtain a median $\text{C IV}/\text{H I} = 2.8 \times 10^{-3}$ and a mean of $\text{C IV}/\text{H I} = [2.4, 2.4] \times 10^{-3}$, similar to the values obtained in Paper I and very slightly higher than those derived from the $\text{Ly}\beta$ -selected sample.

If the $N(\text{C IV})$ threshold is raised to 10^{12} cm^{-2} we detect 41 out of 67 clouds, or $(61 \pm 9)\%$, compared to 17 out of 33, or $(52 \pm 13)\%$, in the Paper I sample. Combining the two data sets we find that 58 out of 100 clouds, or $(58 \pm 8)\%$, are detected above $N(\text{C IV}) = 10^{12} \text{ cm}^{-2}$.

3.4. Detection fractions

In Fig. 6 we show the fraction of clouds detected in C IV as a function of the variable $x \equiv N(\text{C IV})_{\text{det}}/N(\text{H I})_{\text{select}}$ for the $\text{Ly}\alpha$ -selected sample, where $N(\text{H I})_{\text{select}} = 3 \times 10^{14} \text{ cm}^{-2}$. Here $N(\text{C IV})_{\text{det}}$ is our detection limit for C IV, which we can arbitrarily adjust above our observational limit, and $N(\text{H I})_{\text{select}}$ is our selection limit for H I. For $N(\text{C IV})_{\text{det}} \geq 10^{12} \text{ cm}^{-2}$ we have used the data of Q1422+231 augmented by the Paper I data, whereas the $N(\text{C IV}) < 10^{12} \text{ cm}^{-2}$ data point is from Q1442+231 alone.

If the column density distribution of H I, $n(N(\text{H I}))$, can be described approximately by a power law over the range $3 \times 10^{14} \text{ cm}^{-2} \leq N(\text{H I}) \leq 10^{17} \text{ cm}^{-2}$, and the distribution function of $\text{C IV}/\text{H I}$ is invariant as a function of $N(\text{H I})$, then the detection fraction is a function only of the single dimensionless variable, x . In this case the detection fractions as a function of x should be identical for the $\text{Ly}\alpha$ and $\text{Ly}\beta$ samples. Fig. 6 illustrates this agreement (the solid line is the $\text{Ly}\beta$ sample), showing that the data is completely consistent with the hypothesis that all clouds are metal-enriched with a distribution function in $\text{C IV}/\text{H I}$ which is invariant to $N(\text{H I})$, at least around these values of $N(\text{H I})$.

We can also use the data to estimate an upper limit to the fraction of clouds between $N(\text{H I}) = 3 \times 10^{14} \text{ cm}^{-2}$ and $1.6 \times 10^{15} \text{ cm}^{-2}$ that can be primordial. If the H I distribution is a power law with $\beta = 1.7$, then 69% of the clouds in an $N(\text{H I}) > 3 \times 10^{14} \text{ cm}^{-2}$ sample will lie in the range $3 \times 10^{14} - 1.6 \times 10^{15} \text{ cm}^{-2}$. (In fact the fraction of lower column density clouds could be higher at these H I column densities because of the more complex shape of $n(N(\text{H I}))$ [Petitjean et al. 1993, Hu et al. 1995].) Of the $(75 \pm 10)\%$ of the $\text{Ly}\alpha$ -selected clouds detected in C IV, 31% will be contained in the $\text{Ly}\beta$ sample in which essentially all clouds are detected in C IV. Of the remaining 69%, at least $(44 \pm 10)\%$ are detected in C IV, so that a minimum of $(63 \pm 14)\%$ of the clouds in this column density range are detected in C IV.

It can be seen from Fig. 6 that if the clouds are all metal-enriched, a complete identification of the $\text{Ly}\alpha$ sample would require a sensitivity limit corresponding to $x = 5 \times 10^{-4}$ or $N(\text{C IV}) \sim 10^{11} \text{ cm}^{-2}$ which would be hard to achieve even for a quasar as luminous as Q1422+231. Similarly, even a 50% identification of an $N(\text{H I}) \geq 10^{14} \text{ cm}^{-2}$ sample would require a sensitivity of $N(\text{C IV}) = 4 \times 10^{11} \text{ cm}^{-2}$. This means that it will remain very difficult to determine unambiguously the fraction of metal-enriched clouds at column densities much below 10^{15} cm^{-2} , and it remains at least conceptually possible that a large fraction of very low $N(\text{H I})$ clouds could be metal-poor or pristine.

4. Ionization Balance

4.1. Introduction

As we showed in the previous section, the $\text{Ly}\alpha$ forest clouds in the $N(\text{H I}) \geq 1.6 \times 10^{15} \text{ cm}^{-2}$ sample are most easily detected in C IV and less so in C II, Si IV, and N V. In

the present section we investigate the ionization ratios in individual clouds with $N(\text{H I}) > 5 \times 10^{14} \text{ cm}^{-2}$. These turn out to have a relatively small spread, which suggests two possibilities. One is that these clouds are highly invariant in both their average metallicity and in their internal properties, in particular the suitably weighted average internal density. Alternatively, they could be very strongly selected from a more heterogeneous population. In section 4.2 we consider the distribution of the average C IV/H I in $N(\text{H I}) \geq 5 \times 10^{14} \text{ cm}^{-2}$ forest clouds, and in section 4.3 we investigate the internal spread of C IV/H I in the velocity components of individual clouds. In section 4.4 we look at the ratios Si IV/C IV, C II/C IV and N V/C IV and how they restrict the possibility of photoionization models, and in section 4.5 we look at the ionization balance based on a larger list of species in several of the strongest clouds. Finally, in section 4.6 we investigate the evolution of the ion ratios, showing that there is a strong increase of Si IV/C IV with redshift, which has important implications for understanding the evolution of the He^+ opacity in the IGM.

4.2. C IV/H I

At sufficiently high redshift we can measure the properties of the Ly α -saturated clouds by tracing down through the Lyman series. We have measured the H I properties of all clouds above $z = 3.135$ in Q1422+231 and all clouds toward Q0014+813 above $z = 2.95$. From these we have chosen all clouds with $N(\text{H I}) > 5 \times 10^{14} \text{ cm}^{-2}$ in Q1422+231 and $N(\text{H I}) > 10^{15} \text{ cm}^{-2}$ in Q0014+813 where the C IV sensitivity is about a factor of two poorer. The properties of these clouds are summarised in Tables 1 and 2. We also summarise in Table 3 the average properties of all the partial Lyman limit systems (PLLSs) in the observed quasars (Songaila 1996). In Fig. 7 we display C IV/H I, averaged over all the velocity components in an individual cloud, for all the objects in Tables 1, 2 and 3. All 8 of the PLLSs are detected. At $10^{17} < N(\text{H I}) < 10^{18} \text{ cm}^{-2}$, the median C IV/H I is 1.3×10^{-4} and the mean is 2.3×10^{-4} .

For $N(\text{H I})$ in the range $10^{15} - 10^{17} \text{ cm}^{-2}$, 14 out of 18 clouds are detected. The mean C IV/H I is 3.5×10^{-3} and the median value is 3×10^{-3} . At $N(\text{H I}) = 5 \times 10^{14} - 10^{15} \text{ cm}^{-2}$, 5 out of 9 clouds are detected, with a median C IV/H I of 2×10^{-3} . The values for the forest clouds are quite similar to those derived in Section 2 but are now free of assumptions about the distribution of H I column densities, at the cost of having a rather reduced sample.

If we assume for the moment that each cloud is homogeneous and photoionized by a metagalactic flux of specified shape, then C IV/H I is a function only of the ionization parameter, Γ (the ratio of the number density of hydrogen ionizing photons to the electron density) and the metallicity in the cloud. In Fig. 7 we show curves of C IV/H I versus $N(\text{H I})$ from Bergeron & Stasinska (1986) for $\Gamma = 10^{-2.7}$, $10^{-1.7}$, and $10^{-0.7}$ and a carbon abundance of 10^{-2} of solar. For $\Gamma = 10^{-2.5} - 10^{-1.5}$ (section 4.4), which provides the best match to the ionization of other species, the carbon abundances are approximately 10^{-2} of solar, though there could be a spread of at least an order of magnitude in individual clouds. It is extremely hard to deviate much from this abundance, and in particular to reduce the carbon abundance, by changing such assumptions as the internal homogeneity of the clouds because C IV/H I is quite insensitive to Γ over this range, and close to its peak value. We will consider this further in section 4.4.

4.3. C IV/H I in individual velocity components

The C IV/H I values of the previous subsection are averaged over the sometimes complex velocity component structure of an absorption line system, and it is important to understand if the small spread in C IV/H I is an artefact of this averaging or if it continues to hold in the individual velocity components of a system. To look further at this we have determined hydrogen column densities in individual velocity components of the systems in Q1422+231

by fitting the high order Lyman lines, where possible, and have compared these with C IV. A detailed description of the individual systems in Q1422+231 may be found in Appendix A.

The stronger H I components in each system contain C IV with C IV/H I between 5×10^{-4} and 1.5×10^{-2} , the majority lying near 3×10^{-3} (Fig. 8a). The bulk of the C IV occurs in these components, with the result that these C IV/H I ratios are very similar to the average values of the previous subsection. Surrounding them at relative velocities as high as 350 km sec^{-1} (Fig. 8b) are components with much higher values of C IV/H I, in the range 10^{-2} to 10^{-1} , the majority being near the latter value.

The presence of very narrow C IV (as in the $z = 3.513$ system) and, more generally, a comparison of the b -values of C IV and those of H I, suggests that much of the broadening even in the strongest H I components is turbulent rather than thermal. This in turn implies that measured H I b -values of $20 - 28 \text{ km sec}^{-1}$ provide a strong upper bound of 50,000 K to the temperature in strong H I components. This upper limit also applies to most of the higher velocity components. At these temperatures, if the ionization balance were governed by collisional ionization, C II would exceed C IV even in a gas cooling from high temperature (e.g. Shapiro & Moore 1976). It would therefore appear that the gas must be predominantly photoionized. The more highly ionized high velocity components must then be one to two orders of magnitude lower in volume density than the higher column density components.

4.4. Ionization balance

In Figs. 9a through 9c we show values of Si IV/C IV, C II/C IV and N V/C IV versus $N(\text{C IV})$ for all measurable systems in the quasar sample for which $N(\text{H I}) > 5 \times 10^{14} \text{ cm}^{-2}$ and the lines of both species lie longward of the Lyman forest. We have also shown (open symbols) the values in the various partial Lyman limit systems.

All the systems (forest and PLLS) are consistent with having Si IV/C IV in the range 0.03 to 0.4. (As we shall discuss in section 4.6, the spread at a given redshift is smaller.) C II/C IV lies between 0.02 and 0.3, except for the strong PLLS system in Q0636+680 for which C II/C IV = 2. Finally, the small number of N V/C IV measurements yield two values of 0.02 and 0.05, and two comparable upper limits. These values are again consistent with the discussion of the broader samples of section 3. Distinguishing by velocity component again gives similar ionization ratios in the strongest H I components.

If we assume that the highest column density component of the optically thin forest clouds can be parameterised by a single value of the ionization parameter, Γ , and that the ionizing spectrum has a specified form, we can determine the ionization parameter from these ion ratios (e.g. Bergeron & Stasinska 1986, Chaffee et al. 1986, Steidel 1990, Donahue & Shull 1991). The C II/C IV value is most useful for this since it is independent of any assumption about abundance and is insensitive to the exact shape of the high-energy end of the ionizing spectrum and, in particular, to whether or not there is a substantial break across the He⁺ edge at 54 eV. Using the CLOUDY code (Ferland 1993) we find that Γ must be in the range $10^{-2.4}$ to $10^{-1.5}$ to produce the observed C II/C IV values, for a $\nu^{-1.5}$ power law; these values are similar to those inferred from higher column density systems in the work referred to above. This last result can also be seen by comparing the values of C II/C IV in the PLLSs with those in the lower column density systems (Fig. 9b).

The high ion ratios are sensitive to the choice of the shape of the high-energy end of the ionizing spectrum; unfortunately this is rendered quite uncertain by the effect of the He⁺ opacity in the IGM and the poorly known relative contributions of galaxies and AGN. We follow Giallongo & Petitjean (1994) by characterising the spectrum as a broken power law, retaining the $\nu^{-1.5}$ slope but dropping the normalization by a factor B at the He⁺ edge. We have then computed a suite of models with the CLOUDY code corresponding to values of

B from 1 to ∞ .

We show the resultant Si IV/C IV ratios versus C II/C IV in Fig. 10, with small symbols denoting $z < 3.1$ and large symbols corresponding to $z > 3.1$. Intriguingly, these models do not provide a good fit for Si/C in a solar abundance ratio (left panel of Fig. 10) but, as with the low metallicity stars in our Galaxy (e.g. Timmes et al. 1996), require an enhancement of 3 in the α -process silicon over the Fe-process carbon (right panel); this suggests a weighting to higher masses in the metal-producing stars. This is the second conclusion of the paper: Si/C ratios in the forest clouds are similar to those in low metallicity stars in our Galaxy — i.e. about a factor of 3 higher than solar.

The high Si IV/C IV values seen in $z > 3.1$ clouds even in systems with small C II/C IV (that is, high ionization) require that the strength of the break be very large in these clouds ($B \geq 100$) to inhibit silicon from moving to higher ionization levels. This in turn means that there are very few He ionizing photons at these redshifts. However, at $z < 3.1$, the data is consistent with a small break strength ($B = 1 - 10$). We shall consider this evolution with redshift in more detail in section 4.6.

All of the N V/C IV values shown in Fig. 9c correspond to $z > 3.1$ systems and the low values are then a necessary consequence of large breaks across the He⁺ edge. The presence of trace amounts of N V does imply that there must be some high energy ionizing photons, or alternatively some high temperature gas in the systems.

4.5. Strong Systems

For the strongest systems ($N(\text{H I}) \geq 5 \times 10^{15} \text{ cm}^{-2}$) in Q1422+231 it is possible to measure a larger suite of lines and also to obtain measurements of, or at least upper limits to, ions that lie in the forest. We summarise in Table 4 our measurements of C II, C III,

C IV, Si II, Si III, Si IV, and N V in these systems. C II and Si II are both low, as is N V, as would be expected from the strongly broken power law spectrum discussed in section 4.4. Si III is slightly weaker than Si IV, consistent with $\log_{10} \Gamma \sim -1.5$, whereas C III/C IV is less than 1.8, which implies that $\log_{10} \Gamma > -2$.

4.6. Si IV/C IV versus redshift

We have searched in an augmented sample, which consists of the quasars discussed above along with Q2000–330 ($z = 3.777$) and Q1623+268 ($z = 2.526$) for all systems having $N(\text{C IV}) \geq 5 \times 10^{12} \text{ cm}^{-2}$ and for which Si IV lies redward of the forest, as well as any system which is present in Si IV and for which C IV lies within our wavelength coverage. Our spectral coverage of the eight quasars provides a sample of 28 such systems after excluding known Lyman limit systems.

We plot Si IV/C IV for these systems as a function of redshift in Fig. 11, with upper limits shown as downward pointing arrows. Below $z = 3.1$, 13 of 14 systems have Si IV/C IV less than 0.1 whereas 13 of 14 systems redward of $z = 3.1$ have Si IV/C IV greater than 0.1. A rank sum test rejects at the 4×10^{-5} level the possibility that the two samples are drawn from the same distribution function.

As we have discussed in section 4.4 the transition most likely arises from the change in ionizing spectrum from one at $z > 3.1$ that has few photons above the He^+ edge to one with an unbroken power law at lower redshift. The transition is very abrupt — a factor of at least ten in the break strength in a redshift interval of less than 0.1; this favors a crossing of the He^+ ionization boundary in the IGM as the reason rather than the other possibility, namely the changeover from a galaxy-dominated ionizing flux at $z > 3.1$ to a quasar-dominated flux at $z < 3.1$.

Si IV/C IV can be related to He II/H I, as we illustrate in Fig. 12 for the power law-break models computed with CLOUDY. At high redshift where Si IV/C IV is large, He II/H I lies between 250 and 2000, depending on Γ , whereas He II/H I should be much lower — around 20 to 40 — at lower redshift ($z < 3.1$).

Kim et al. (1996) have shown recently that the number density evolution of high and low column density clouds is quite distinct over this redshift range: unlike high column density clouds, which show rapid evolution, the number density of $N(\text{H I}) < 3 \times 10^{14} \text{ cm}^{-2}$ clouds is invariant and described by a $\beta \approx -1.5$ power law. It is these low column density clouds that provide the dominant contribution of the forest to the He II opacity. If we assume that the same metagalactic flux ionizes both low and high column density clouds, then there will be an abrupt drop in the He II opacity at $z \sim 3.1$, with relatively constant values above and below this redshift. The drop in the opacity varies as $(\text{He II}/\text{H I})^{0.5}$ for a $\beta = -1.5$ power law (Miralda-Escudé 1993) and so will lie between 2.5 and 10, depending on typical values of Γ in the clouds. This could explain the discrepancy between the value of $\tau_{\text{He II}} \gg 1.7$ measured at $z \leq 3.286$ (Jakobsen et al. 1994) and the much lower $\tau_{\text{He II}} = 1$ found by Davidsen et al. (1996) at $z \leq 2.72$.

5. Proximate Systems

The interpretation of the relative deficiency of Ly α clouds close to a quasar’s redshift (the proximity effect) as being caused by the ionization of the quasar itself (Bajtlik, Duncan & Ostriker 1988, Lu, Wolfe & Turnshek 1991) predicts that clouds within a few thousand km sec^{-1} of the quasar should have significantly higher ionization parameters than clouds in the general field. This effect should be more pronounced for high ion ratios at $z > 3.1$ as we have argued that the metagalactic ionizing flux at high redshift is severely

deficient in high energy photons.

We have searched for this effect in our values of C IV/H I and Si IV/C IV, as is shown in Fig. 13 where we plot all clouds with $N(\text{C IV}) > 10^{12} \text{ cm}^{-2}$. The cloud closest to Q1422+231 is indeed highly anomalous. This system in Q1422+231 shows unsaturated Ly α , extremely strong C IV and N V but very weak Si IV and C II. We show the spectra of Ly α , C IV, Si IV and N V in Fig. 14; the absorption consists of two roughly equal components separated by 53 km sec^{-1} whose properties are summarized in Table 5.

The very low values of Si IV/C IV (< 0.007 and 0.013 respectively) require a power-law ionization with a relatively small break at the He $^+$ edge; this of course is what is expected if the cloud is directly exposed to the quasar’s ionizing flux. For a $\nu = -1.5$ power law, $\log_{10} \Gamma = -1.75$ and -1.5 produce good fits to the ionization ratios in the two components. However, with these values of the ionization parameter, the observed C IV/H I of 0.35 and 0.5 require an approximately solar metallicity in the cloud, suggesting that it might be associated with the quasar rather than lying in the general IGM.

The simplicity of the component structure in this system also allows us to test the temperature prediction of the photoionization models. Predicted b -values versus atomic weight are shown in Fig. 15 with temperature computed both with low metallicity (dotted line) and with solar metallicity. In order to fit the observed trend in b , we must introduce a substantial turbulent broadening equivalent to $b = 14 \text{ km sec}^{-1}$ in each component.

6. The C IV Correlation Function

Fernandez-de Soto et al. (1996) have recently analyzed the C IV line systems given in Paper I and find a strong correlation signal in the C IV absorption lines at small velocity separations. The present Q1422+231 data set provides a somewhat better determination of

this. In Figure 16 we show the two-point correlation function (TPCF) of C IV absorption lines with $N(\text{C IV}) > 10^{12} \text{ cm}^{-2}$ and $2.66 < z < 3.62$. The shape and strength of the correlation function are relatively insensitive to the column density cut. The correlation function is slightly weaker than Fernandez-de Soto et al. find but it is in broad agreement with the results of Womble, Sargent & Lyons (1996) who analyzed independent data on Q1422+231.

There is a very weak anticorrelation at $\Delta v > 300 \text{ km sec}^{-1}$ so it is not possible to measure a large scale correlation signal with this data, and the observed correlation at $\Delta v < 300 \text{ km sec}^{-1}$ is subject to the usual uncertainties introduced by the internal velocity dispersions, effective sizes, and geometries of the objects. Moreover, it is clear from the discussion of section 4.3 that C IV has a more extended velocity distribution in a given line system than H I, and so the Ly α correlation function will have a weaker amplitude than that of C IV.

We fitted the TPCF with the functional form of Heisler, Hogan & White (1989)

$$\xi(\nu) = \frac{1}{(2\pi)^{1/2}} \int_{r_{cl}}^{\infty} \frac{H dr}{\sigma} \left(\frac{r}{r_{corr}} \right)^{-\gamma} \left[\exp -\frac{(Hr - \nu)^2}{2\sigma^2} + \exp -\frac{(Hr + \nu)^2}{2\sigma^2} \right] \quad (1)$$

where $H(z)$ is the Hubble constant at redshift z , σ is the velocity dispersion of the clouds, r_{cl} is the cloud dimension and r_{corr} is the correlation length. The distances are in physical (proper) units. For $q_0 = 0.5$, the best fit, shown as the dashed line in Fig. 15, has $r_{corr} \approx 270h^{-1} \text{ kpc}$, $\sigma = 100 \text{ km sec}^{-1}$, and $r_{cl} = 40h^{-1} \text{ kpc}$, where $h = (H_0/100 \text{ km sec}^{-1})$. For comparison, Christiani et al. (1995) found $r_{corr} = 280h^{-1} \text{ kpc}$, $\sigma = 150 \text{ km sec}^{-1}$, and $r_{cl} = 110h^{-1} \text{ kpc}$ for the Ly α correlation. If we *assume* that ξ corresponds to the galaxy correlation function and evolves as

$$\xi = (1 + z)^{-3-\epsilon} \left(\frac{r}{r_0} \right)^{-1.8} \quad (2)$$

where $r_0 = 5.5h^{-1} \text{ Mpc}$ is the current galaxy correlation length, then $\epsilon \sim 1$, which is slightly

weaker than the $\epsilon = 2.4$ found by Fernandez-de Soto et al. but still denotes a relatively fast evolution in the galaxy correlation function, such as might be found in an $\Omega = 1$ universe.

7. Conclusion

We can summarise the conclusions fairly simply. Lyman forest clouds with $N(\text{H I}) > 10^{15} \text{ cm}^{-2}$ are ubiquitously metal-enriched, typically having carbon abundances 10^{-2} of solar and Si/C of about three times solar, values very similar to those of Galactic halo stars. At $N(\text{H I})$ below 10^{15} cm^{-2} , current sensitivity limits for $N(\text{C IV})$ are inadequate to determine whether or not all clouds have C IV if the distribution function of C IV/H I is similar to that at higher column density. The data are perfectly consistent with the clouds having the same distribution function but could permit as many as half of the clouds with $3 \times 10^{14} < N(\text{H I}) < 10^{15} \text{ cm}^{-2}$ to be chemically pristine.

We have investigated the ionization in the $N(\text{H I}) > 5 \times 10^{14} \text{ cm}^{-2}$ clouds and shown that they have relatively uniform properties with a spread of at most an order of magnitude in their metallicities and ionization parameters, the latter lying between $\Gamma = 10^{-2.4}$ and $\Gamma = 10^{-1.5}$. The one exception is the single cloud lying closer than 1000 km sec^{-1} to a quasar, in which the metallicity is near solar. The clouds are structured in velocity, and the highest velocity components are more highly ionized, which suggests that we are seeing layered structure in an individual system such as might be formed in a pancake collapse. This internal structure may be responsible for the two point velocity correlation which is seen at $\Delta v < 300 \text{ km sec}^{-1}$. Alternatively, if the velocity correlation is interpreted in terms of the galaxy correlation function we find a relatively rapid evolution of this quantity from $z = 3$ to $z = 0$.

Finally, and perhaps most intriguingly, we find that there is a rapid evolution in the

value of Si IV/C IV at a redshift of about 3.1 which we interpret as being caused by a change in the spectrum of the metagalactic ionizing flux, which must go from having a strong break at the He⁺ edge at $z > 3.1$ to having a weak break at $z < 3.1$. This could be a result of the transition from a galaxy-dominated to a quasar-dominated ionizing flux, but, given the rapidity of the transition, it appears to be more likely that we are seeing the He⁺ ionization boundary in the intergalactic medium. Irrespective of the origin of the effect, the evolution of the ionizing spectrum implies that we will observe much weaker He⁺ edges in quasar spectra at redshifts $z < 3.1$.

A. Structure of Individual Systems in Q1422+231

Velocities are measured relative to the strongest H I component.

3.264: C IV consists of one single broad line with $N(\text{C IV}) = 4 \times 10^{12} \text{ cm}^{-2}$ and a b -value of 19 km sec^{-1} . It corresponds to a hydrogen line with $N(\text{H I}) = 1.7 \times 10^{15} \text{ cm}^{-2}$ and $b = 28 \text{ km sec}^{-1}$. The separation of the centroids of C IV and H I is $+3 \text{ km sec}^{-1}$.

3.410: C IV consists of a stronger wide component with $b = 22 \text{ km sec}^{-1}$ and $N(\text{C IV}) = 8 \times 10^{12} \text{ cm}^{-2}$ centered at $+1 \text{ km sec}^{-1}$ from the strongest H I with $N(\text{H I}) = 1.8 \times 10^{15} \text{ cm}^{-2}$ and $b = 26 \text{ km sec}^{-1}$. There is a weaker wing with $b = 14 \text{ km sec}^{-1}$ and $N(\text{C IV}) = 2 \times 10^{18} \text{ cm}^{-2}$ at -47 km sec^{-1} from the main hydrogen component, which appears to correspond to a blueward wing in the H I at -43 km sec^{-1} from the main component. $N(\text{H I}) = 1.8 \times 10^{14} \text{ cm}^{-2}$ and $b = 21 \text{ km sec}^{-1}$ in this wing.

3.499: There is a wide C IV line with $b = 19 \text{ km sec}^{-1}$ and $N(\text{C IV}) = 2 \times 10^{12} \text{ cm}^{-2}$ at $+7 \text{ km sec}^{-1}$ from the H I with $b = 26 \text{ km sec}^{-1}$ and $N(\text{H I}) = 2.7 \times 10^{15} \text{ cm}^{-2}$. The C IV column density is somewhat insecure because of neighboring lines in the region of C IV $\lambda 1548 \text{ \AA}$.

3.513: The C IV consists of two narrow components with $b = 7 \text{ km sec}^{-1}$ and $N(\text{C IV}) = 7 \times 10^{12} \text{ cm}^{-2}$ and $b = 12 \text{ km sec}^{-1}$, $N(\text{C IV}) = 3 \times 10^{12} \text{ cm}^{-2}$ at -5 km sec^{-1} and $+20 \text{ km sec}^{-1}$ respectively from the hydrogen line with $N(\text{H I}) = 1.8 \times 10^{15} \text{ cm}^{-2}$ and $b = 24 \text{ km sec}^{-1}$. Their weighted mean lies $+3 \text{ km sec}^{-1}$ redward of the neutral hydrogen.

3.536: This high column density system is extremely complex. There are 8 main C IV clouds: (-329 km sec^{-1} , $b = 17 \text{ km sec}^{-1}$, $N(\text{C IV}) = 6 \times 10^{12} \text{ cm}^{-2}$), (-264 km sec^{-1} , $b = 22 \text{ km sec}^{-1}$, $N(\text{C IV}) = 4.4 \times 10^{13} \text{ cm}^{-2}$), (-172 km sec^{-1} , $b = 10 \text{ km sec}^{-1}$, $N(\text{C IV}) = 8 \times 10^{12} \text{ cm}^{-2}$), (-107 km sec^{-1} , $b = 15 \text{ km sec}^{-1}$, $N(\text{C IV}) = 10^{13} \text{ cm}^{-2}$), (-86 km sec^{-1} , $b = 11 \text{ km sec}^{-1}$, $N(\text{C IV}) = 4.3 \times 10^{13} \text{ cm}^{-2}$), (-43 km sec^{-1} , $b = 13 \text{ km sec}^{-1}$, $N(\text{C IV}) = 4.6 \times 10^{13} \text{ cm}^{-2}$), (2 km sec^{-1} , $b = 21 \text{ km sec}^{-1}$, $N(\text{C IV}) = 6 \times 10^{12} \text{ cm}^{-2}$), (92 km sec^{-1} , $b = 4 \text{ km sec}^{-1}$, $N(\text{C IV}) = 10^{12} \text{ cm}^{-2}$) as well as a further $3 \times 10^{13} \text{ cm}^{-2}$ distributed more uniformly. The strongest neutral hydrogen component has $N(\text{H I}) = 1.2 \times 10^{16} \text{ cm}^{-2}$ and $b = 22 \text{ km sec}^{-1}$, but there are further strong components at negative velocities: (-263 km sec^{-1} , $b = 34 \text{ km sec}^{-1}$, $N(\text{C IV}) = 6.4 \times 10^{15} \text{ cm}^{-2}$), (-232 km sec^{-1} , $b = 18 \text{ km sec}^{-1}$, $N(\text{C IV}) = 2.0 \times 10^{15} \text{ cm}^{-2}$), (-177 km sec^{-1} , $b = 22 \text{ km sec}^{-1}$, $N(\text{C IV}) = 6.2 \times 10^{15} \text{ cm}^{-2}$), (-106 km sec^{-1} , $b = 46 \text{ km sec}^{-1}$, $N(\text{C IV}) = 3.4 \times 10^{15} \text{ cm}^{-2}$). The four systems that have both C IV and H I identified from profile fitting (-263 km sec^{-1} , -177 km sec^{-1} , -106 km sec^{-1} , and 0 km sec^{-1}) have C IV/H I = 6.9×10^{-3} , 1.3×10^{-3} , 3×10^{-3} , and 5×10^{-4} respectively. Neutral hydrogen is quite weak in the extreme velocity components: $N(\text{H I}) = 7 \times 10^{13} \text{ cm}^{-2}$ at -329 km sec^{-1} for C IV/H I = 9×10^{-2} , and $N(\text{H I}) = 2 \times 10^{13} \text{ cm}^{-2}$ for C IV = 5×10^{-2} at $+92 \text{ km sec}^{-1}$. The two intermediate components at -86 km sec^{-1} and -43 km sec^{-1} are more uncertain but consistent with as much as $N(\text{H I}) = 4 \times 10^{14} \text{ cm}^{-2}$ in each.

3.565: This system consists of a single C IV line with $b = 13 \text{ km sec}^{-1}$ and $N(\text{C IV}) = 1.4 \times 10^{12} \text{ cm}^{-2}$ separated by $+4 \text{ km sec}^{-1}$ from the $N(\text{H I}) = 2.5 \times 10^{15} \text{ cm}^{-2}$ and $b =$

21 km sec⁻¹ neutral hydrogen line.

3.586: The main C IV component with $b = 23$ km sec⁻¹ and $N(\text{C IV}) = 1.6 \times 10^{13}$ cm⁻² lies at +3 km sec⁻¹ from the neutral hydrogen line with $b = 28$ km sec⁻¹ and $N(\text{H I}) = 4.2 \times 10^{15}$ cm⁻². In addition there is a probable second component with $b = 21$ km sec⁻¹ and $N(\text{C IV}) = 4 \times 10^{12}$ cm⁻² at +144 km sec⁻¹ from this position. (The agreement between the doublets is not as precise as usual, and there is a possibility that this component is spurious.) There is only a weak Ly α feature near this velocity, with $b = 22$ km sec⁻¹ and $N(\text{H I}) = 3.3 \times 10^{13}$ cm⁻². The C IV line lies at +3 km sec⁻¹ from this line.

REFERENCES

- Batjlik, S., Duncan, R. C. & Ostriker, J. P. 1988, *ApJ*, 327, 570.
- Bergeron, J. & Ikeuchi, S. 1990, *AA*, 235, 8.
- Bergeron, J. & Stasinska, G. 1986, *AA*, 169, 1.
- Cen, R. Y., Miralda-Escudé, J., Ostriker, J. P. O. & Rauch, M. 1994, *ApJ*, 437, L9.
- Chaffee, F. H., Foltz, C. B., Bechtold, J. & Weymann, R. J. 1986, *ApJ*, 301, 116.
- Cristiani, S., D’Odorico, S., Fontana, A., Giallongo, E. & Savaglio, S. 1995, *MNRAS*, 273, 1016.
- Cowie, L. L., Songaila, A., Kim, T.-S. & Hu, E. M. 1995 *AJ*, 109, 1522 (Paper I).
- Davidson, A. F., Kriss, G. A. & Zheng, W. 1996, *Nature* 380, 47.
- Donahue, M. & Shull, J. M. 1991, *ApJ*, 383, 511.
- Ferland, G. J. 1993, University of Kentucky Department of Physics and Astronomy Internal Report.
- Fernandez-de Soto, A., Lanzetta, K. M., Barcons, X., Carswell, R. F., Webb, J. K. & Yahil, A. 1996, *ApJ*, 460, L85.
- Giallongo, E. & Petitjean, P. 1994, *ApJ*, 426, L61.
- Haehnelt, M. G., Steinmetz, M. & Rauch, M. 1996, submitted to *ApJ*.
- Heisler, J., Hogan, C. & White, S. D. M. 1989, *ApJ*, 347, 52.
- Hu, E. M., Kim, T.-S., Cowie, L. L., Songaila, A. & Rauch, M. 1995, *AJ*, 110, 1526.
- Jakobsen, P. et al. 1994, *Nature*, **370**, 35.
- Kim, T.-S., Hu, E. M., Cowie, L. L. & Songaila, A. 1996, in preparation.
- Lu, L. Wolfe, A. M., & Turnshek, D. A. 1991, *ApJ*, 367, 19.

- Miralda-Escudé, J. 1993, MNRAS, 262, 273.
- Petitjean, P., Webb, J. K., Rauch, M., Carswell, R. F. & Lanzetta, K. 1993, MNRAS, 262, 499.
- Petitjean, P., Rauch, M. & Carswell, R. F. 1994, AA, 291, 29.
- Rees, M. J. 1995, in *QSO Absorption Lines*, ESO Astrophysics Symposia, ed. G. Meylan (Berlin: Springer), p. 419.
- Sargent, W. L. W., Boksenberg, A. & Steidel, C. C. 1988, ApJS, 68, 539.
- Shapiro, P. & Moore, 1976, ApJ, 207, 460.
- Songaila, A., Cowie, L. L. & Lilly, S. J. 1990, ApJ, 348, 371.
- Songaila, A., 1996, in preparation.
- Songaila, A. Hu, E. M. & Cowie, L. L. 1995, *Nature*, **375**, 124.
- Steidel, C. C. 1990, ApJS, 74, 37.
- Timmes, F. X., Lavroesch, J. T. & Truran, J. W. 1996, ApJ, in press.
- Tytler, D., et al. 1995, in *QSO Absorption Lines*, ESO Astrophysics Symposia, ed. G. Meylan (Heidelberg: Springer), p. 289.
- Womble, D. S., Sargent, W. L. W. & Lyons, R. S., 1996, to appear in *Cold Gas at High Redshift*, eds. M. Bremer, H. Rottgering, G. P. VanderWerf & C. Carilli (Dordrecht: Kluwer).
- Yee, H. K. C. & Ellingson, E. 1994, *Astr. J.*, **107**, 28.
- Zhang, Y., Anninos, P. & Norman, M. L. 1995, ApJ, 453, L57.

We are grateful to T. Bida, R. Campbell, P. Gillingham, J. Aycok, T. Chelminiak, B. Shaeffer and W. Wack for their extensive help in obtaining the observations and to E. Hu and K. Roth who carried out parts of the observing. We would like to thank P. Jakobsen and M. Shull for comments on an earlier draft of this paper and Michael Rauch and Ray Weymann for helpful discussions.

TABLES

TABLE 1 — C IV Lines in Q1422+231 for $N(\text{H I}) > 5 \times 10^{14} \text{ cm}^{-2}$ Systems

TABLE 2 — C IV Lines in Q0014+813 for $N(\text{H I}) > 10^{15} \text{ cm}^{-2}$ Systems

TABLE 3 — Partial Lyman Limit Systems

TABLE 4 — Strong Systems in Q1422+231

TABLE 5 — Proximate System

Fig. 1.— The spectrum of Q1422+231. The bottom panel shows a complete spectrum, while the upper is a 100 Å region redward of the quasar’s Ly α emission. The data have been two-point smoothed. This spectrum was obtained on 1995 July 2,3 and August 5 using three settings of the HIRES echelle spectrograph on the Keck telescope; the total exposure was 8.33 hours. The data were reduced as described in Paper I and Hu et al. 1995. The spectrum has a resolution, $R = 36,000$, and provides complete wavelength coverage from 3900 Å to 7200 Å. At the C IV region shown, the S/N is measured as 160 per resolution element. 31 C IV systems containing 66 velocity components can be identified in the C IV region longward of the Lyman forest ($z = 2.66 - 3.63$).

Fig. 2.— Atlas of 62 L α -saturated clouds in Q1422+231 for $z > 2.65$. In each case we show the L α line (bottom), then the L β line (for systems with $z > 2.92$), and then the C IV $\lambda 1548$ Å and C IV $\lambda 1550$ Å lines (top). The observed air redshift is shown in the left corner.

Fig. 3.— A 100 Å portion of the spectrum of Q1422+231 (bottom) with the corresponding L β (middle) and C IV $\lambda 1548$ Å (top) shifted in wavelength so they lie above L α . Dotted vertical lines indicate clouds that are saturated in both L β and L α . Short dotted lines show the position of C IV $\lambda 1550$ Å corresponding to these clouds.

Fig. 4.— (a) Column densities of C IV corresponding to all Lyman forest systems with saturated $L\beta$ in numerous quasar lines of sight. These are — Q0014+813: $z = 2.84 - 3.30$; Q0256–000: $z = 2.79 - 2.86$; Q0302–003: $z = 2.74 - 2.86$; Q0636+680: $z = 2.64 - 2.74$; Q0956+122: $z = 2.75 - 2.92$; Q1159+123: $z = 2.95 - 3.05$; Q1206+119: $z = 2.60 - 2.85$; Q1422+231: $z = 2.92 - 3.60$; Q2126–158: $z = 2.73 - 3.00$. Detected C IV systems are shown at the measured column density but all undetected systems are shown at a nominal value of 10^{12} cm^{-2} . Throughout the figures, absorption lines toward Q1422+231 are shown as diamonds, those toward Q0014+813 as triangles, and the remainder as squares. (b) As in (a) for Si IV; undetected systems are shown at $5 \times 10^{11} \text{ cm}^{-2}$. (c) As in (a) for N V; undetected systems are shown at 10^{12} cm^{-2} . (d) As in (a) for C II; undetected systems are shown at 10^{12} cm^{-2} .

Fig. 5.— $N(\text{C IV})$ versus redshift for $\text{Ly}\alpha$ saturated clouds in Q1422+231. The solid line shows the adopted detection limit of $5 \times 10^{11} \text{ cm}^{-2}$.

Fig. 6.— The detected fraction of clouds versus the parameter $x \equiv N(\text{C IV})_{det}/N(\text{H I})_{select}$, where $N(\text{C IV})_{det}$ is the detection limit for C IV and $N(\text{H I})_{select}$ is the selection limit in $N(\text{H I})$. The filled squares and diamonds show the detection fraction for the $\text{Ly}\alpha$ -selected sample [$N(\text{H I})_{select} \approx 3 \times 10^{14} \text{ cm}^{-2}$] with $\pm 1\sigma$ error bars, whereas the solid line shows the result for the $\text{Ly}\beta$ -selected sample [$N(\text{H I})_{select} \approx 1.6 \times 10^{15} \text{ cm}^{-2}$].

Fig. 7.— C IV versus H I column density for all systems with $N(\text{H I}) > 5 \times 10^{14} \text{ cm}^{-2}$ at $3.135 < z < 3.60$ toward Q1422+231(diamonds) and for $N(\text{H I}) \geq 1.5 \times 10^{15} \text{ cm}^{-2}$ at $z > 2.95$ toward Q0014+813 (triangles). Also shown (open squares) are detected C IV/H I values in all PLLSs toward the eight quasars (Songaila 1996). The dashed line shows the typical 2σ detection limit for C IV in Q1422+231. The solid lines show model calculations (Bergeron & Stasinska 1986) of C IV/H I for $\Gamma = 10^{-2.7}$ (lower), $\Gamma = 10^{-1.7}$ (upper) and the dotted line the model for $\Gamma = 10^{-0.7}$, and a metallicity of 10^{-2} solar, and illustrate that the difference between the PLLS and lower column density systems is not solely a radiative transfer effect but must arise from a higher ionization parameter or higher metallicity in the weaker clouds.

Fig. 8.— (a) C IV/H I versus H I for the components described in Appendix A. (b) C IV/H I versus velocity separation from the strongest H I component in each absorption line system.

Fig. 9.— Si IV/C IV, C II/C IV and N V/C IV as a function of C IV for all L β saturated systems where the lines lie redward of the forest and within the wavelength coverage (filled squares). The solid lines are 2σ detection limits for Q1422+231. Upper limits for the other quasar lines of sight are shown with downward pointing arrows. We have also shown values for the PLLSs (open squares).

Fig. 10.— Comparison of the observed values of Si IV/C IV versus C II/C IV with model predictions of the CLOUDY code. The models are computed for a $\nu^{-1.5}$ power law with various breaks across the He⁺ edge (dashed line — no break; dotted line — factor of 2; dash-dot line — factor of 10; long dash line — factor of 100; solid line — factor of 1000) and for two values of Si/C (left panel — solar; right panel — low metallicity, Si/C = 3 times solar).

Fig. 11.— Si IV/C IV versus redshift for all clouds with $N(\text{C IV}) \geq 5 \times 10^{12} \text{ cm}^{-2}$ that are not known Lyman limit systems and for which Si IV lies longward of the Lyman alpha forest. (Downward pointing arrows are 1σ upper limits.) The filled diamonds are values for Q1422+231 and the filled triangles for Q0014+813. The squares are from the sample of quasars of Table 1, augmented at the lowest redshift by observations of Q1623+269 (open squares) and at the higher redshifts with Q2000–330, which are shown by the open triangles. The tick marks show the redshifts below which He^+ edge breaks have been measured (Jakobsen et al. 1994, Tytler et al. 1995, Davidsen et al. 1996). The optical depth measured by Davidsen et al. (1996) at $z = 2.743$ is much lower ($\tau = 1$) than that measured by Jakobsen et al. (1994) at $z = 3.286$ ($\tau \gg 1.7$); these redshifts roughly bracket the epoch at which Si IV/C IV values drop abruptly.

Fig. 12.— He II/He I versus Si IV/C IV for the CLOUDY models of Fig. 10. We assume here the low metallicity ratio for Si/C.

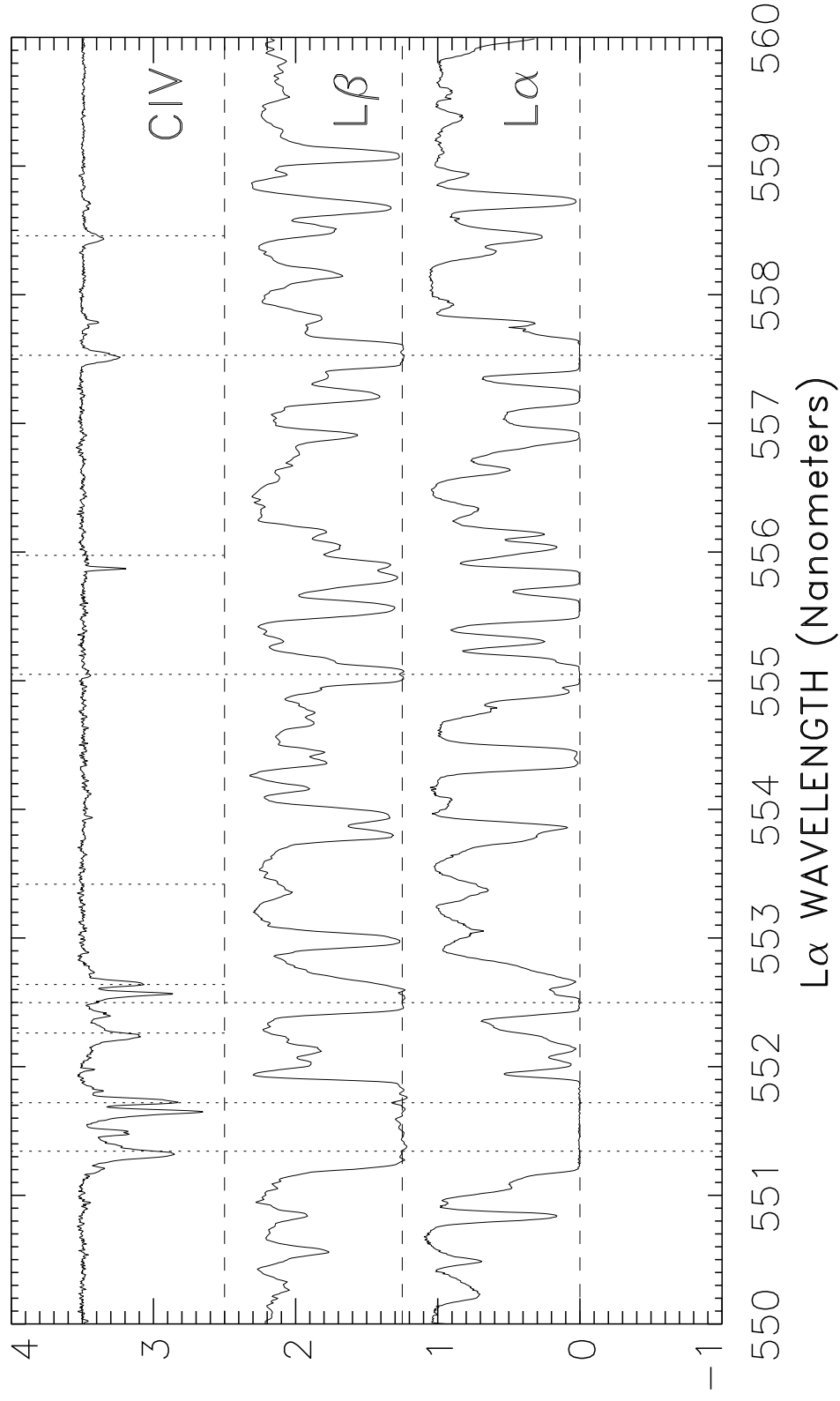
Fig. 13.— (a) C IV/H I and (b) Si IV/C IV versus separation velocity from the quasar for all clouds with $N(\text{C IV}) > 10^{12} \text{ cm}^{-2}$. Clouds toward Q1422+231 are shown as diamonds, and clouds toward Q0014+813 are shown as triangles.

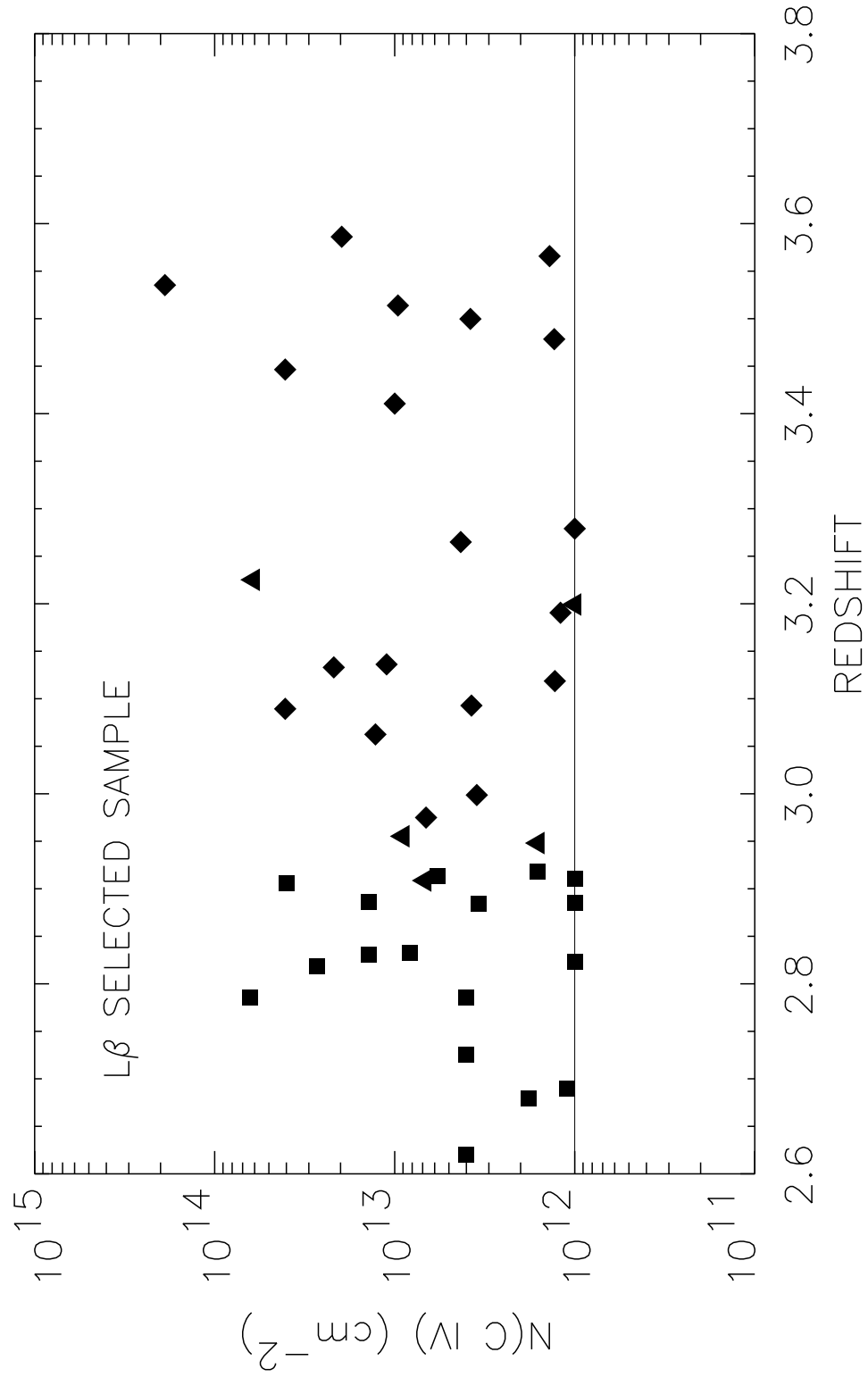
Fig. 14.— Line profiles for the proximate system at $z = 3.623$ in the spectrum of Q1422+231. The bottom spectrum is $\text{Ly}\alpha$ with above (in order) C IV ($\lambda 1548 \text{ \AA}$), C IV ($\lambda 1550 \text{ \AA}$), Si IV ($\lambda 1393 \text{ \AA}$), Si IV ($\lambda 1402 \text{ \AA}$), N V ($\lambda 1238 \text{ \AA}$), N V ($\lambda 1242 \text{ \AA}$).

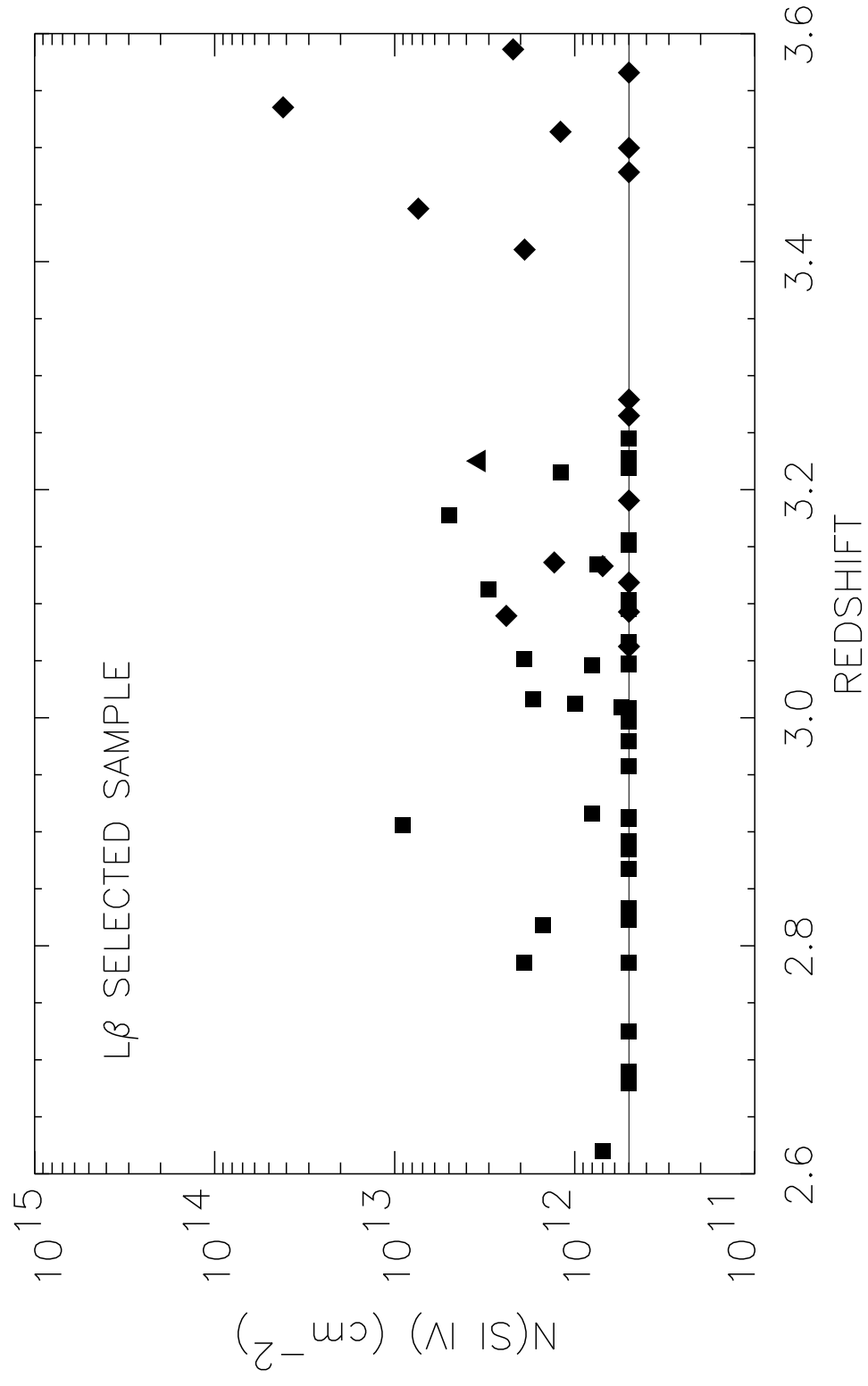
Fig. 15.— b -value versus atomic weight for the two velocity components of the system of Fig. 13 ($\text{Ly}\alpha$, C IV and N V) are shown as squares. The dotted and dashed lines show model predictions for the thermal broadening at temperatures predicted by the CLOUDY models for low metallicity (dotted) and solar metallicity (dashed). The solid line includes a further turbulent component with $b = 14 \text{ km s}^{-1}$.

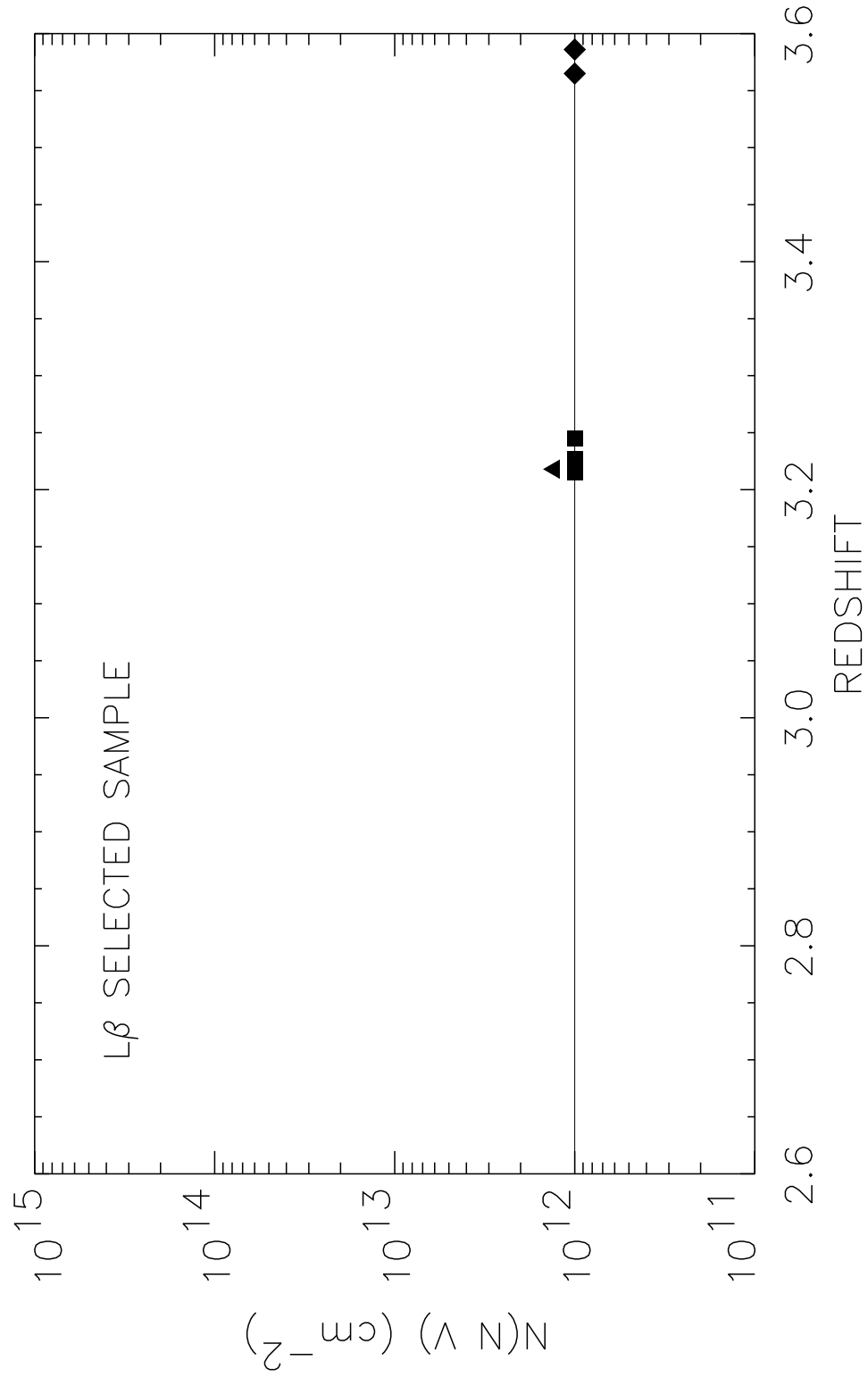
Fig. 16.— The two-point velocity correlation function of the 52 C IV lines with $N(\text{C IV}) \geq 3 \times 10^{12} \text{ cm}^{-2}$ toward Q1422+231, excluding the partial Lyman limit system. The correlation function is shown in 50 km s^{-1} bins with 1σ error bars based on the number of pairs in each bin.

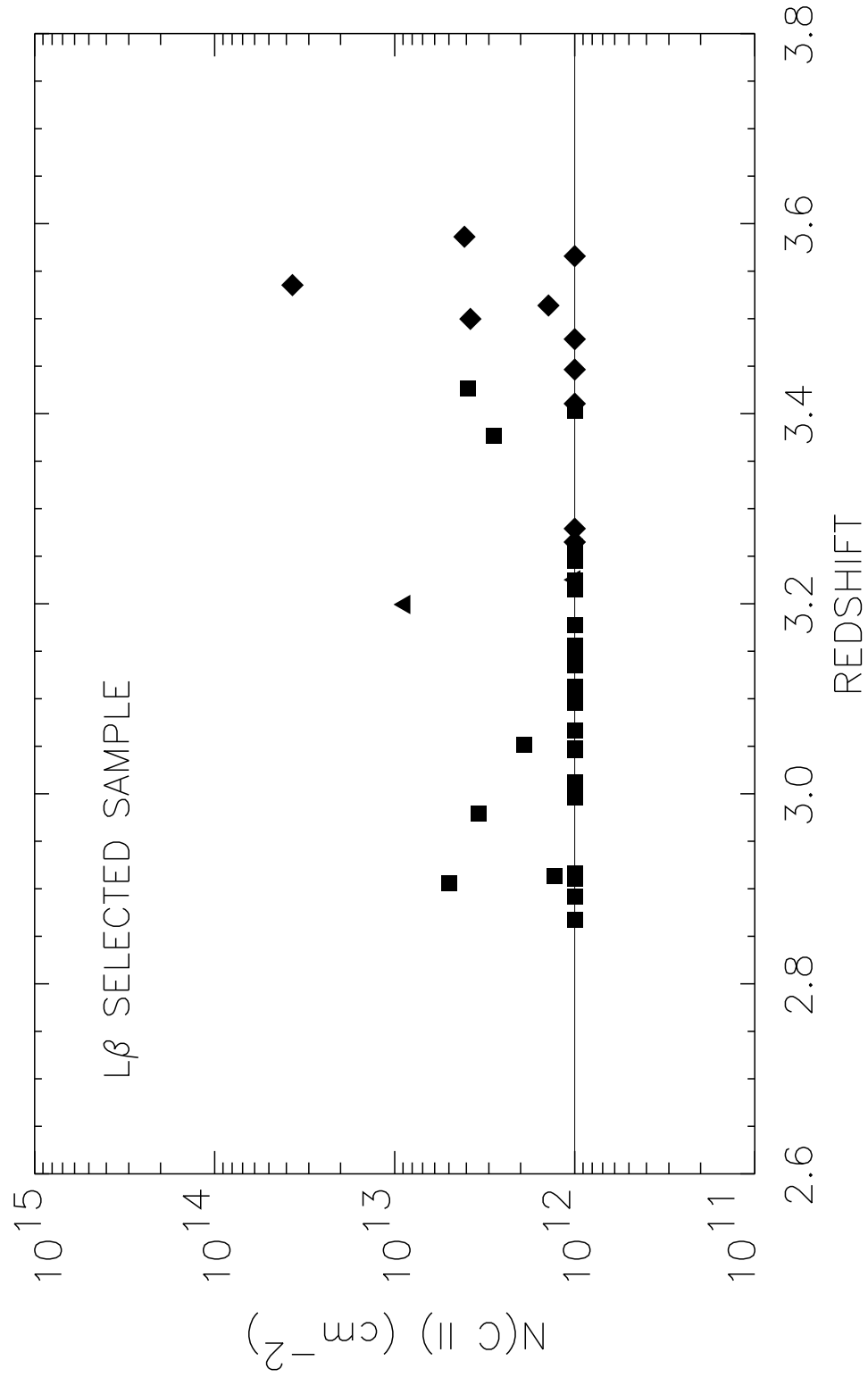
Q1422+231

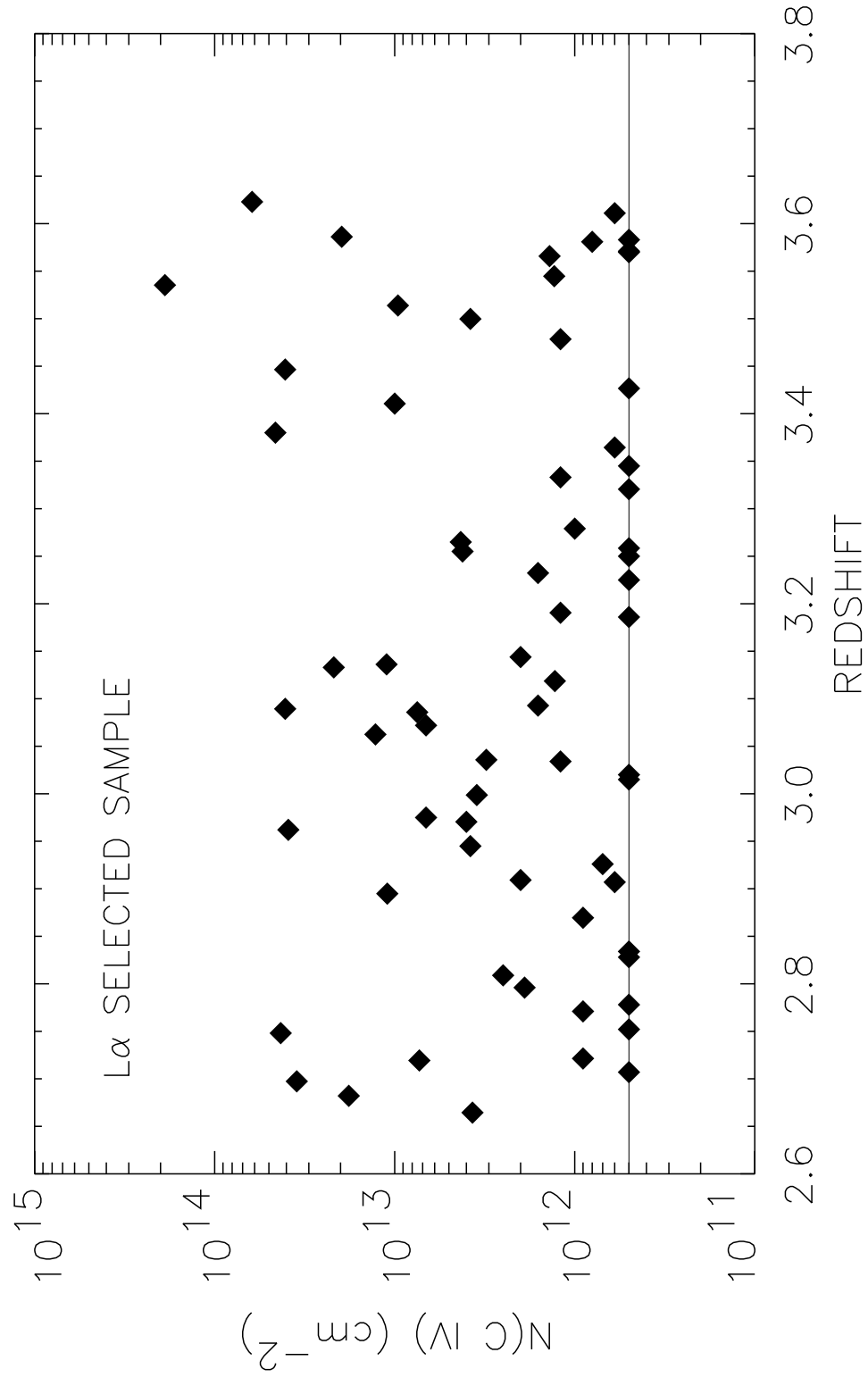


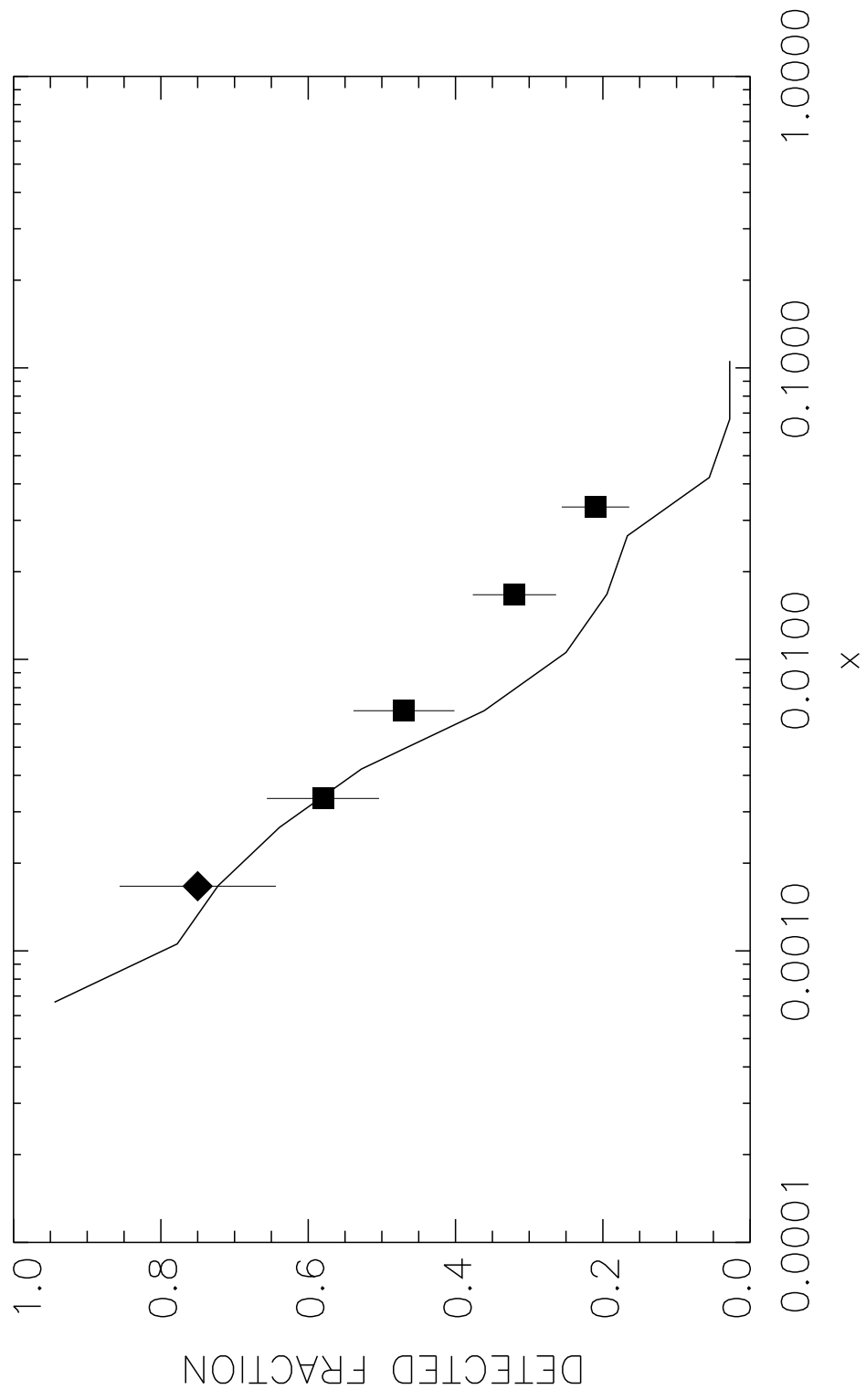


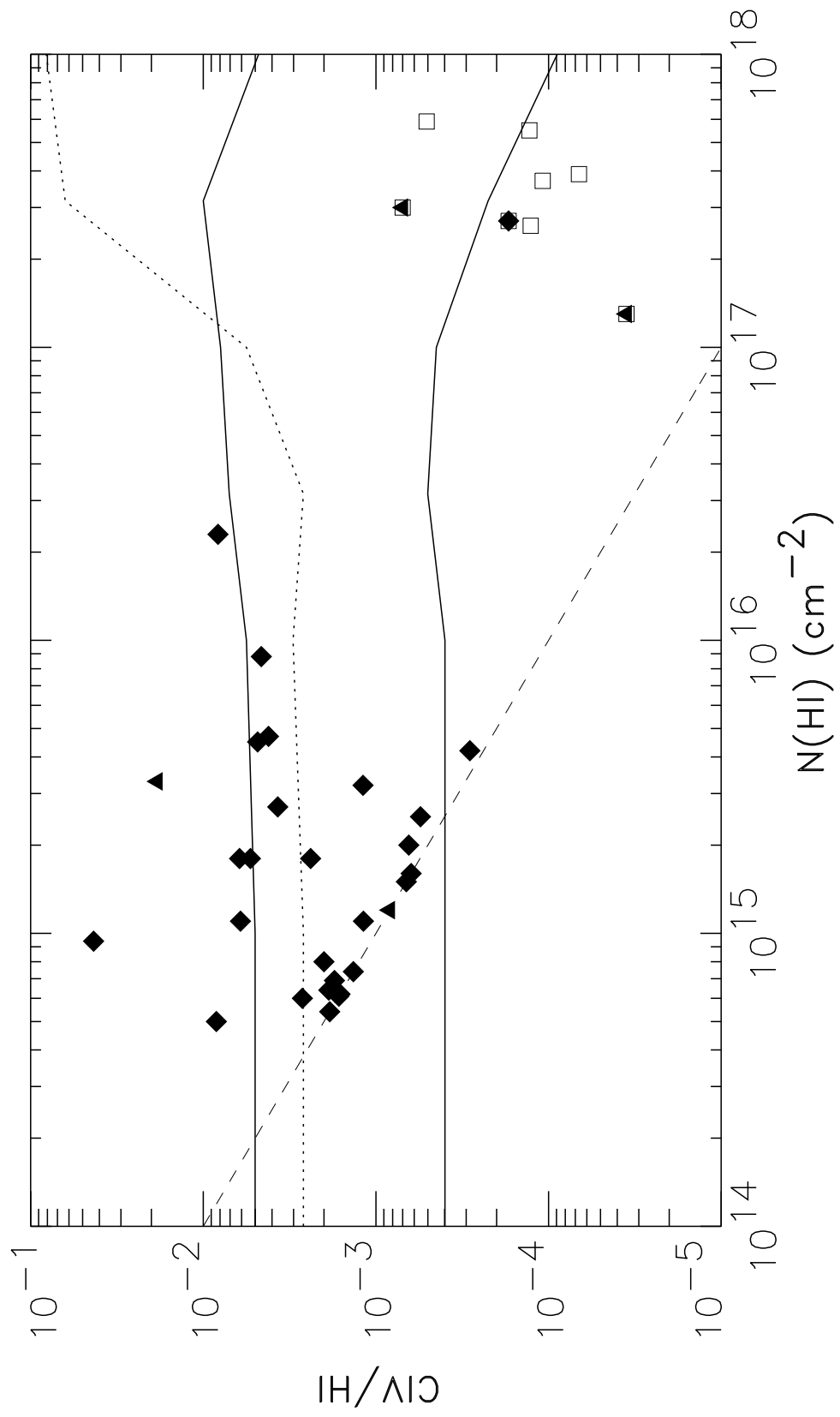


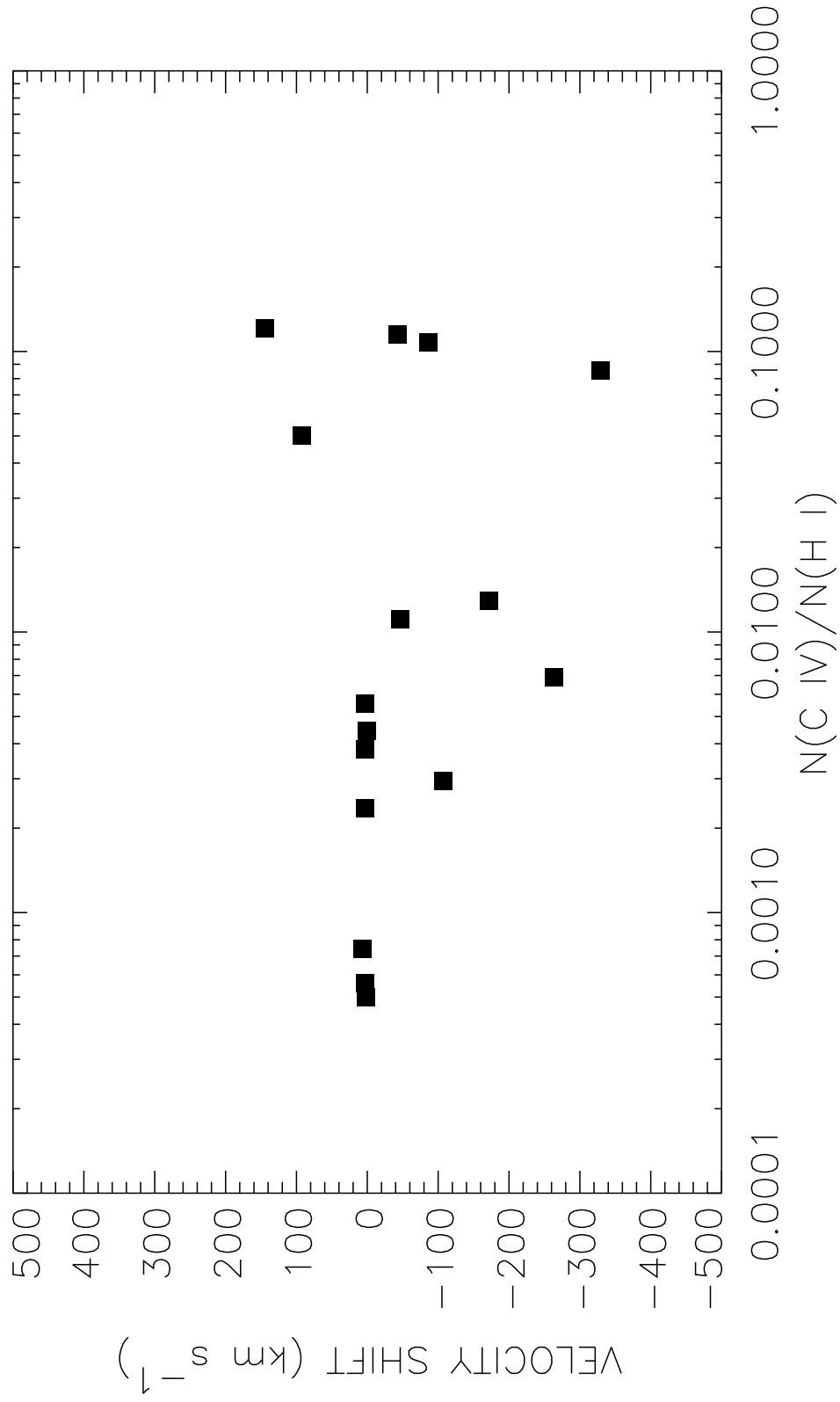


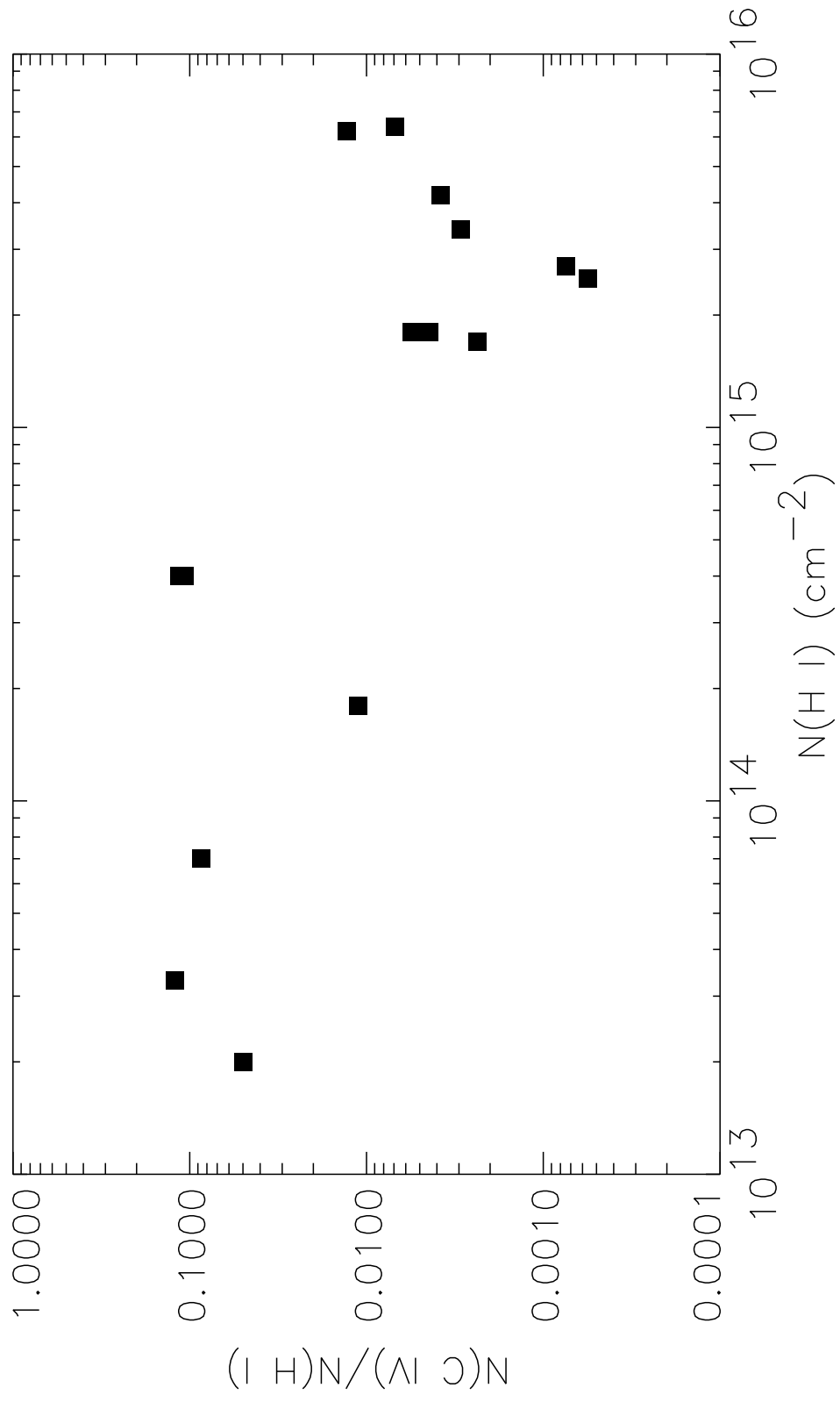


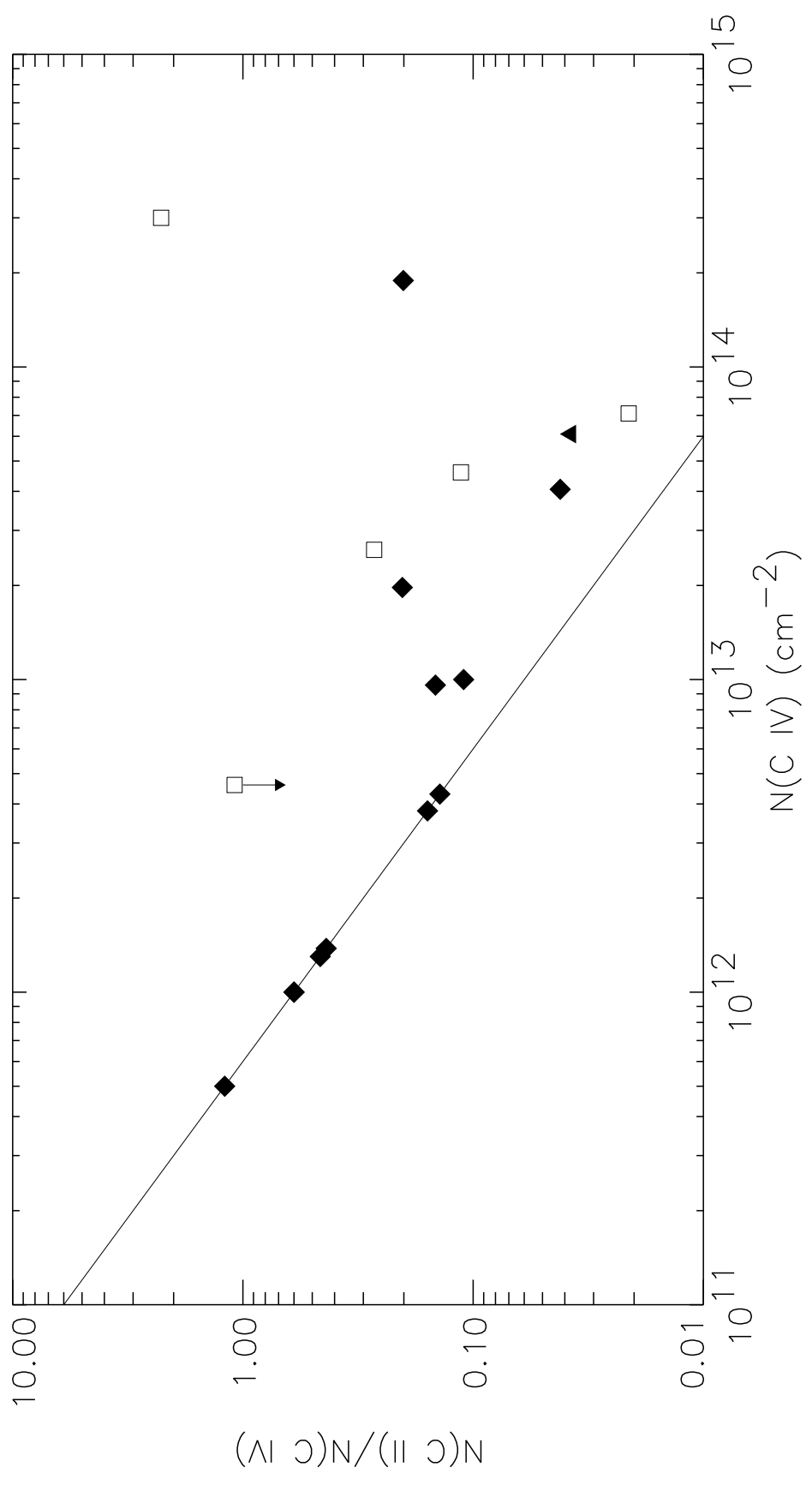


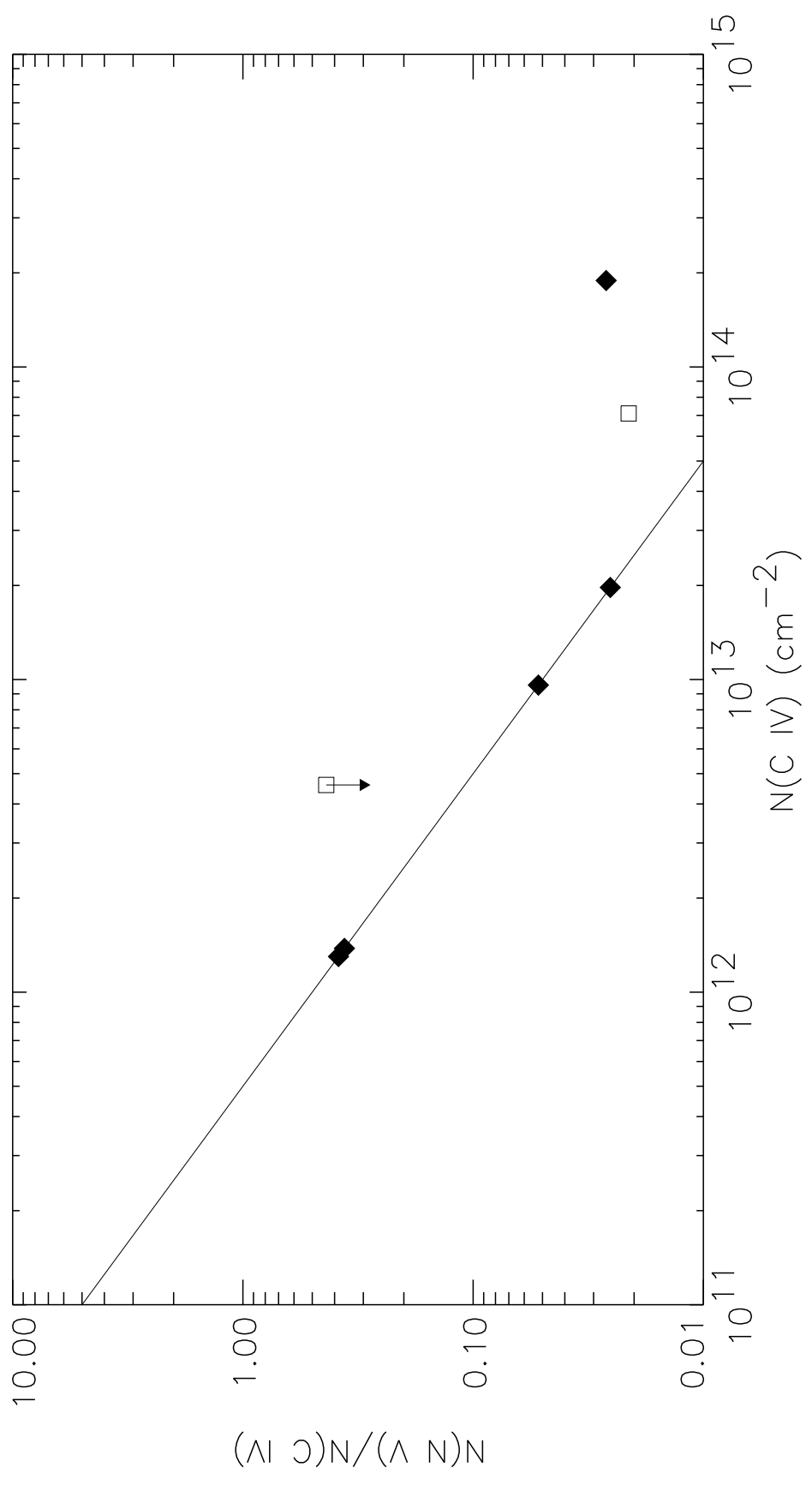


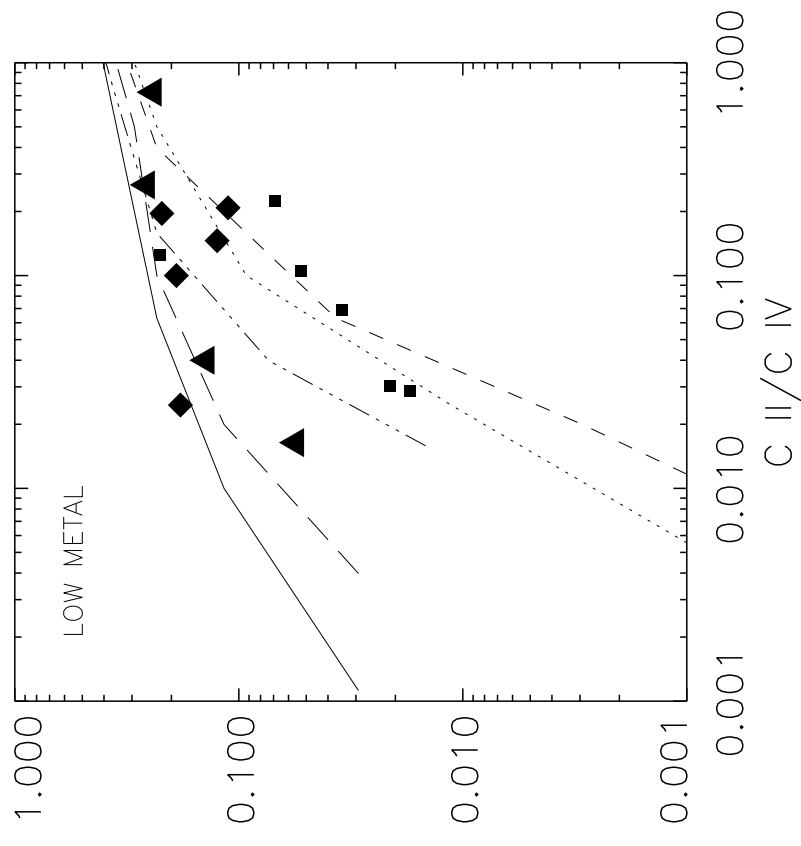
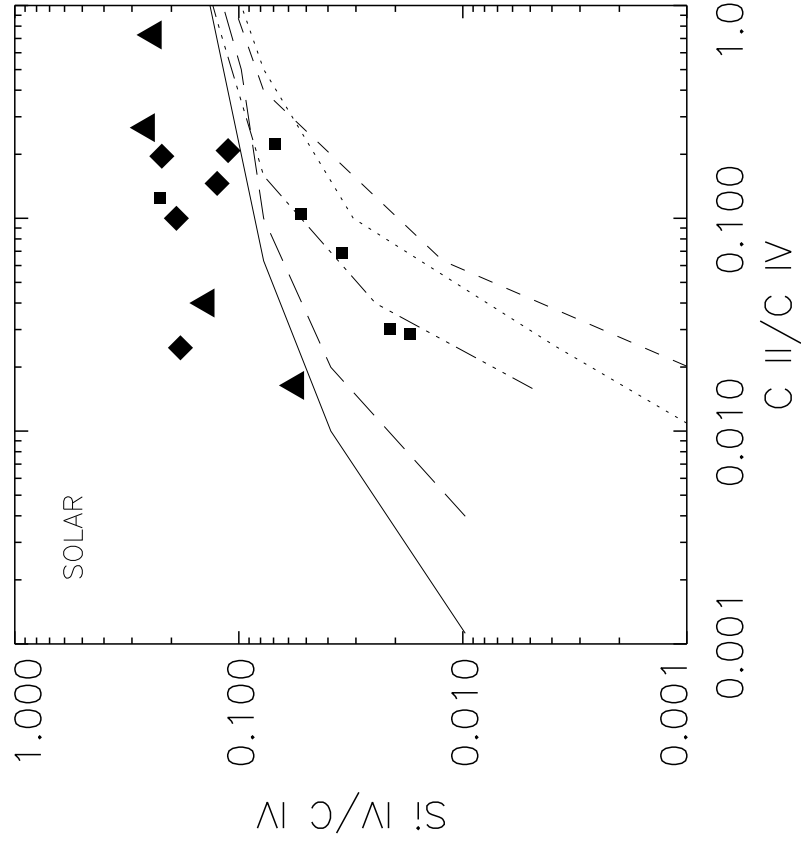


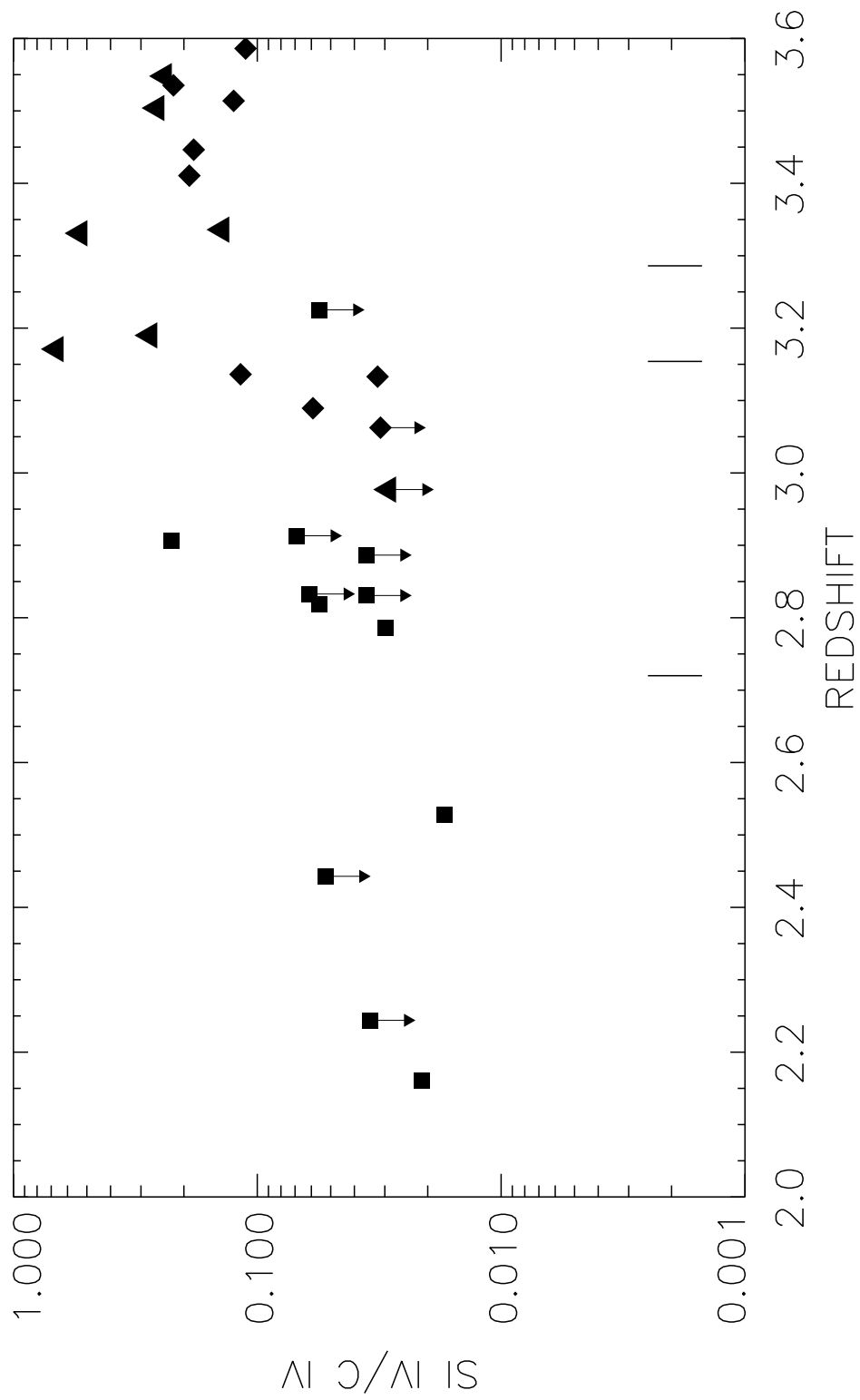


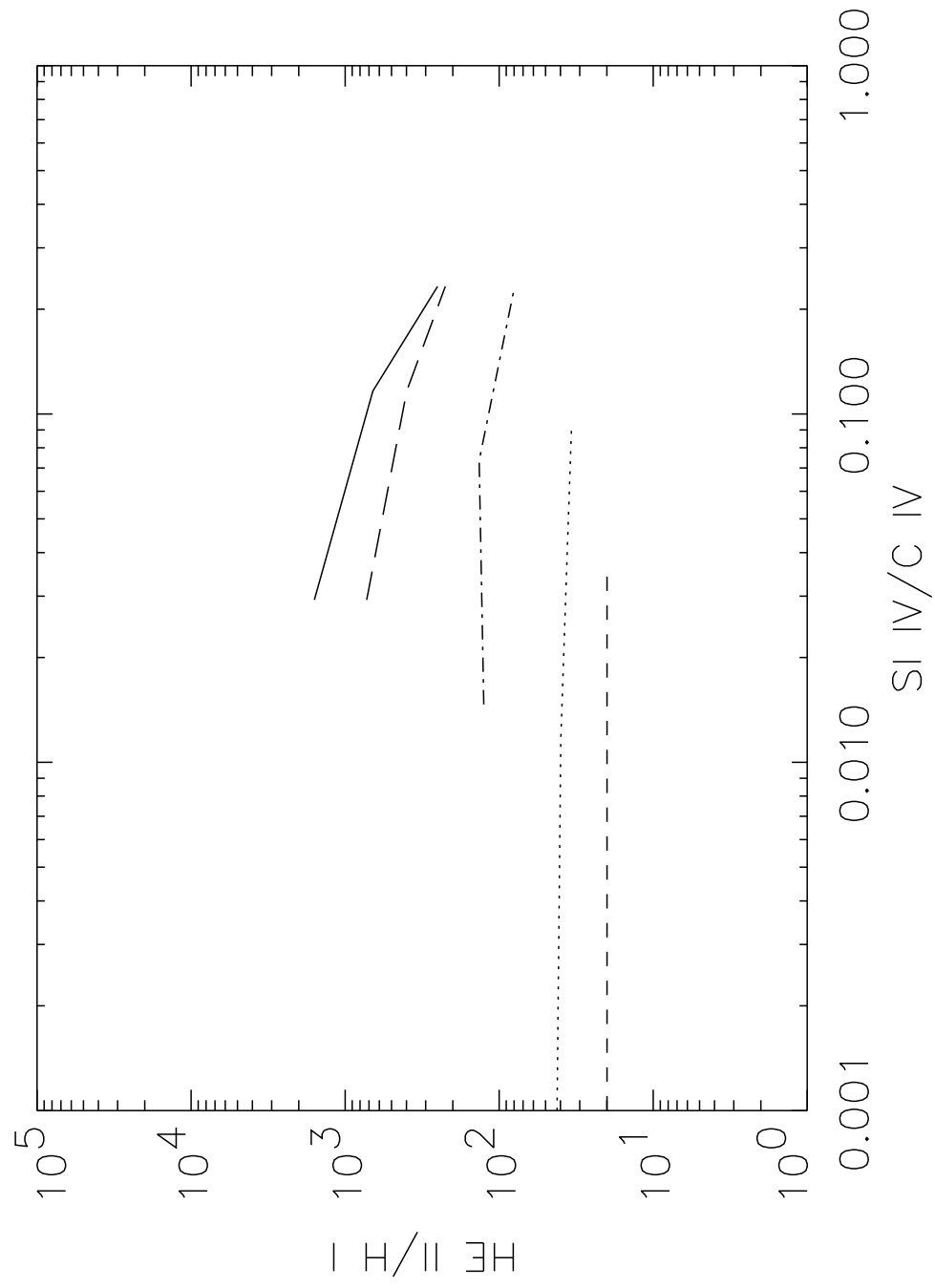


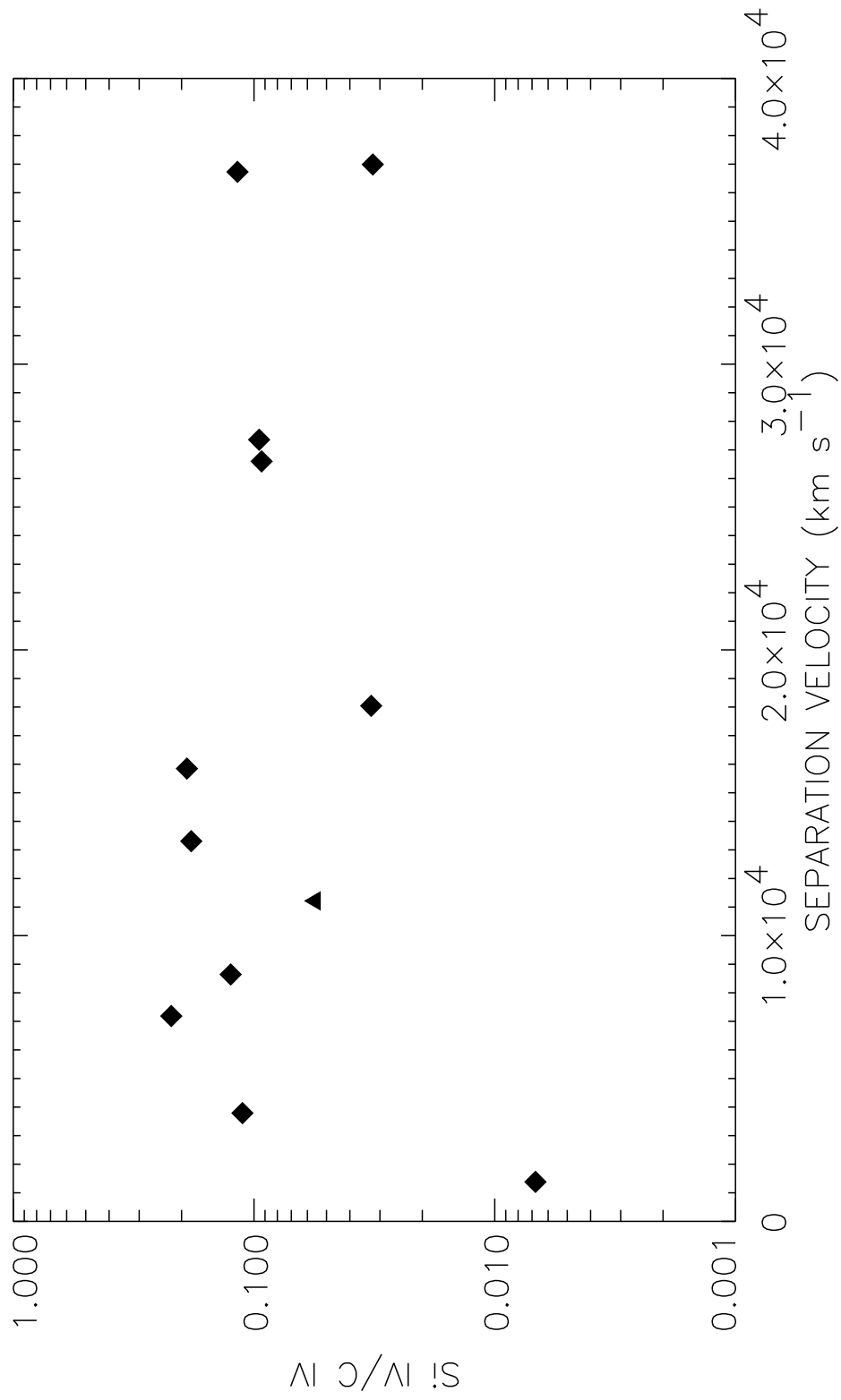


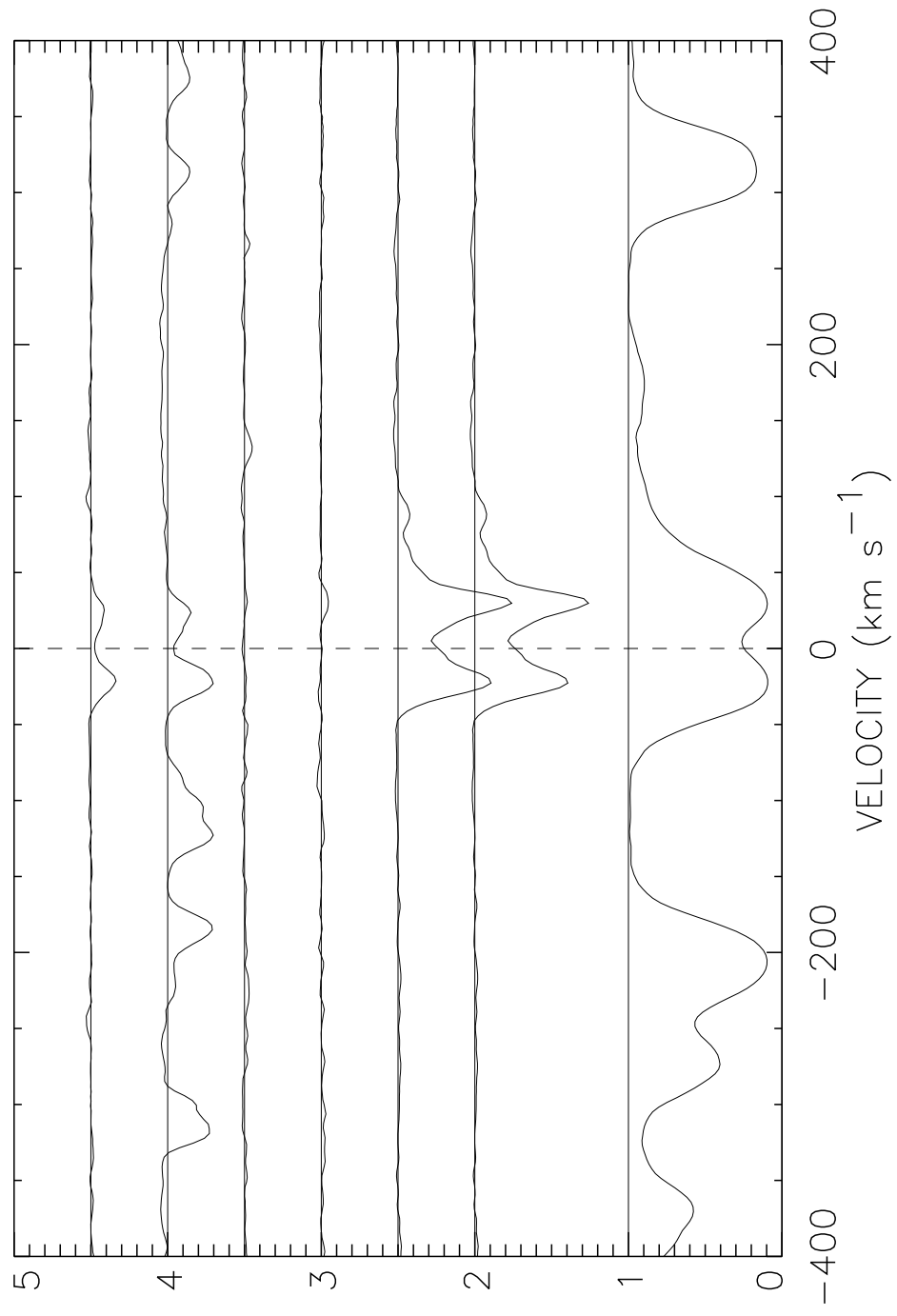


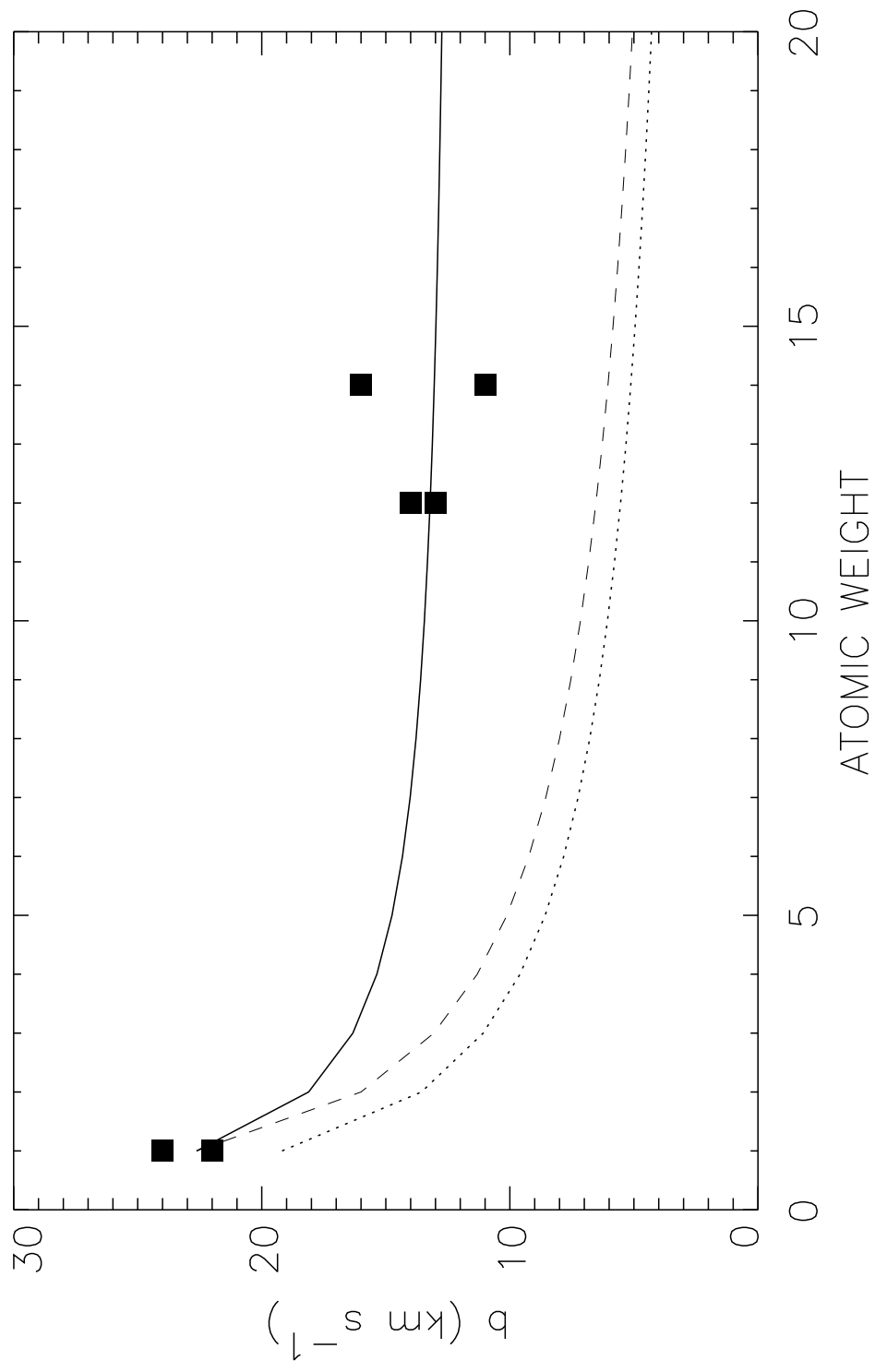












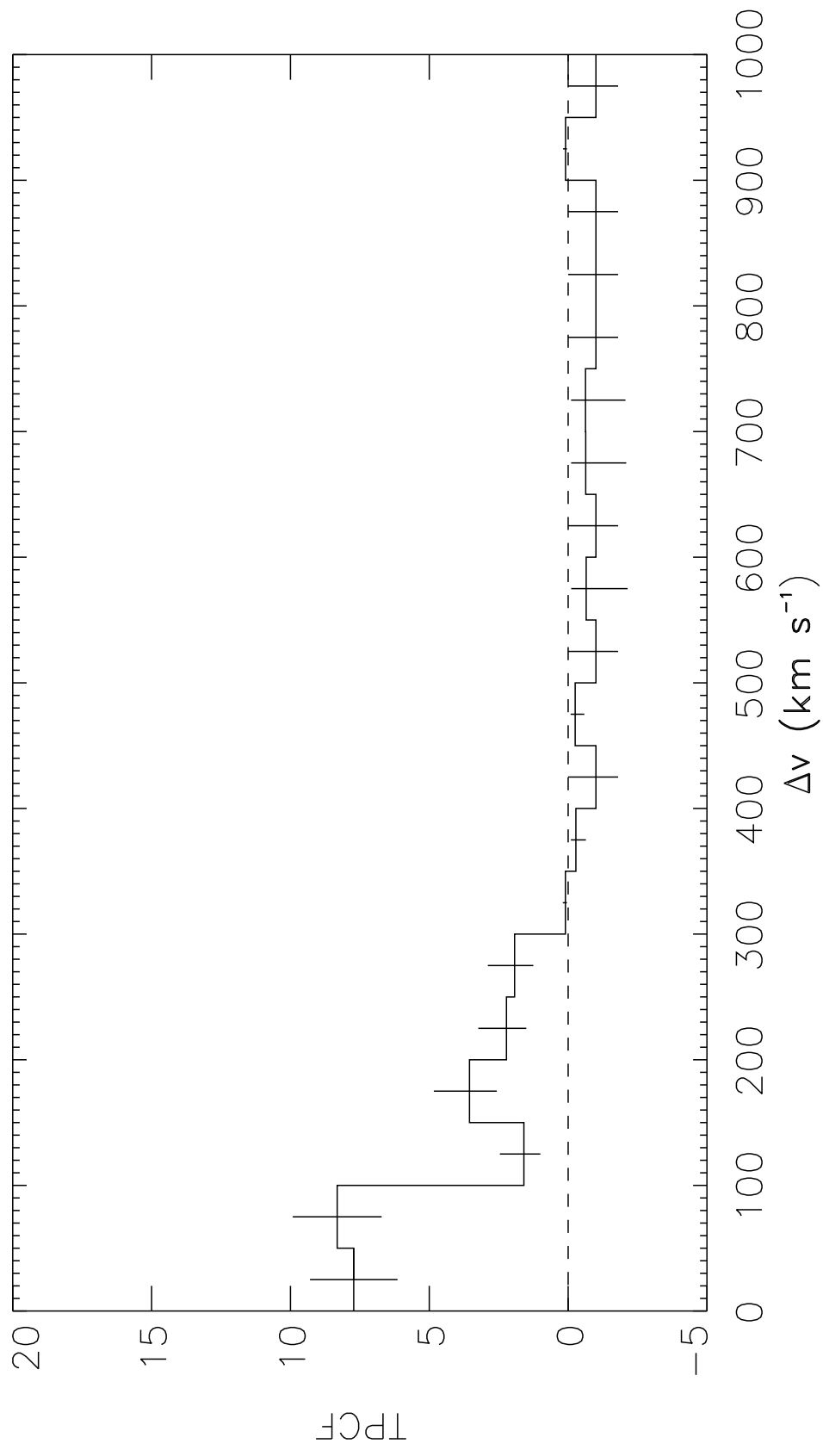


TABLE 1. C IV Lines in Q1422+231 for $N(\text{H I}) > 5 \times 10^{14} \text{ cm}^{-2}$ Systems

z	$N(\text{H I})$ (cm^{-2})	$v(\text{C IV})$ (km s^{-1})	$b(\text{C IV})$ (km s^{-1})	$N(\text{C IV})$ ($\times 10^{12} \text{ cm}^{-2}$)
3.5862	4.7×10^{15}	-5	23	15.6
		137	21	4.2
3.5710	5.4×10^{14}	—	—	—
3.5699	6.2×10^{14}	—	—	—
3.5658	2.5×10^{15}	2	13	1.4
3.5447	1.1×10^{15}	-3	6	1.3 :
3.5353	2.3×10^{16}	-74	31	10.2
		-16	18	34.3
		-5	8	4.5
		17	35	23.8
		80	15	15.2
		151	25	20.5
		167	10	37.9
		210	14	37.9
		257	20	6.5
3.5139	1.8×10^{15}	17	12	3.1
		-7	7	6.5
3.4997	2.7×10^{15}	4	22	2.1
3.4785	4.2×10^{15}	0	8	1.2
3.4463	8.8×10^{15}	-28	7	8.1
		0	12	32.6
3.4105	2.7×10^{15}	-144	14	1.9
		4	22	8.0
3.3809	1.5×10^{17}	-22	24	1.0
		-117	36	6.8
		-6	12	17.5
		34	14	16.7
		68	8	3.6
3.3330	6.9×10^{14}	10	12	1.3
3.3202	6.1×10^{14}	-21	6	0.7
3.2790	1.6×10^{15}	-3	10	0.4
3.2649	1.8×10^{15}	-7	23	4.3
3.2509	7.4×10^{14}	—	—	—
3.2323	6.0×10^{14}	10	11	1.6
3.2253	1.5×10^{15}	-10	6	0.5
3.1905	6.6×10^{14}	8	7	1.2
3.1362	1.8×10^{15}	6	18	7.8
		72	34	3.3
3.1330	4.4×10^{15} :	-82	20	3.0

TABLE 1. (continued)

z	$N(\text{H I})$ (cm^{-2})	$v(\text{C IV})$ (km s^{-1})	$b(\text{C IV})$ (km s^{-1})	$N(\text{C IV})$ ($\times 10^{12} \text{ cm}^{-2}$)
		6	27	9.7
		48	14	9.1
3.1186	2.0×10^{15} :	23	6	1.3
3.0928	8.0×10^{14}	0	9	1.6 :
3.0894	9.4×10^{14}	-20	11	7.1
		11	30	23.9
		64	9	8.5
3.0717	1.1×10^{15}	-100	19	6 :
		0	6	0.7 :

TABLE 2. C IV Lines in Q0014+813 for $N(\text{H I}) > 10^{15} \text{ cm}^{-2}$ Systems

z	$N(\text{H I})$ (cm^{-2})	$v(\text{C IV})$ (km s^{-1})	$b(\text{C IV})$ (km s^{-1})	$N(\text{C IV})$ ($\times 10^{12} \text{ cm}^{-2}$)
3.3209	1.3×10^{17}	38	20	4.6
3.2253	1.2×10^{15}	-50	11	4.1
		-37	10	5.9
		-15	7	14.0
		11	14	7.7
		28	7	6.5
		76	20	19.1
3.1992	1.3×10^{15}	—	—	—

TABLE 3. Partial Lyman Limit Systems

QSO	z	H I ^(a) $\times 10^{17}$	C IV $\times 10^{13}$	Si IV $\times 10^{13}$	C II $\times 10^{12}$	Si II $\times 10^{12}$	Si III $\times 10^{13}$	C III $\times 10^{13}$	N V $\times 10^{12}$
0014+813	2.7989	3.0	21.0	4.3	—	9.0	< 6.0	—	—
—	3.3213	1.3	0.46	< 0.15	< 5.0	< 0.5	0.13	—	< 2.0
0256+000	3.0829	3.6	4.0	1.5	—	< 1.0	< 2.0	—	< 20.0
0302–003	2.5341	2.6	3.3	0.36	—	< 0.8	1.0	—	—
0636+680	2.9031	5.9	30.0	13.0	680.0 ^(b)	83.0	14.0	—	—
0956+122	3.2216	5.5	7.1	1.4	< 1.5	0.3	1.2	—	< 1.5
1422+231	3.3809	2.7	4.6	0.15	5.2	< 0.8	—	< 4.5	—
2126–158	2.9661	3.9	2.6	0.39	7.0	—	< 0.4	—	—

^(a)All column densities in cm^{-2} .

^(b) $n_{\text{tot}} < 0.05 \text{ cm}^{-3}$ based on C II*.

TABLE 4. Strong Systems in Q1422+231

Line	$z = 3.5353$	$z = 3.4464$	$z = 3.5862$
H I	2.3×10^{16}	8.8×10^{15}	5.1×10^{15}
C II	3.8×10^{13}	$< 1.5 \times 10^{12}$	4.0×10^{12}
C III	—	$\leq 7.5 \times 10^{13}$	$\leq 3.5 \times 10^{13}$
C IV	1.9×10^{14}	4.1×10^{13}	1.9×10^{13}
Si II	4.5×10^{12}	$< 8 \times 10^{11}$	$\leq 4 \times 10^{11}$
Si III	3.9×10^{13} :	4.8×10^{12} :	$\leq 6.4 \times 10^{12}$
Si IV	4.1×10^{13}	7.4×10^{12}	2.1×10^{12}
N V	$< 5 \times 10^{12}$	—	$< 2 \times 10^{12}$

Si III is in the Lyman forest but the feature appears to be a metal line, based on line position and width.

TABLE 5. Proximate System

Q1422+231 ($z = 3.623$)		
	-20 km s^{-1}	$+33 \text{ km s}^{-1}$
H I	8.0×10^{13}	7.1×10^{13}
C IV	2.8×10^{13}	3.5×10^{13}
Si IV	$< 2.0 \times 10^{11}$	5×10^{11}
N V	1.6×10^{13}	1.2×10^{13}
C II	$< 5.0 \times 10^{11}$	$< 5.0 \times 10^{11}$
C II*	—	—